Multi-Particle Spectral Densities
Mehrteilchen-Beiträge zu spektralen Dichten

Sebastian Kirschner

Diplomarbeit

Institut für Theoretische Physik
Universität zu Köln

Juni 2004

Contents

Chapter 1

Zusammenfassung

In dieser Arbeit werden die 3-Teilchen Beiträge der Spektraldichte der Spin-1/2 Leiter für verschiedene Verhältnisse der Kopplungsstärken von Holm- zu Sprossenkopplung $x \in \{0.25, 0.5, 0.75, 1.0\}$ und Gesamtspin $S = 0$ untersucht. Für verschwindende Holmkopplung $x = 0$ zerfällt die Leiter in isolierte Dimere bzw. Sprossen. Die vier Eigenzustände eines Dimers sind ein Singulett und drei Tripletts. Das Singulett liegt energetisch tiefer als die drei Tripletts. Der Hamiltonoperator lässt sich in einen in der Dimer-Basis diagonalen Sprossenanteil und einen nicht-diagonalen Holmanteil aufspalten. Durch eine kontinuierliche unitäre Transformation lässt sich ein in der Kopplung x pertubativer Hamiltonoperator gewinnen, der die Zahl der Anregungen erhält. Die Triplettanregungen der Dimere werden durch die Transformation zu Tripletts, die mit Polarisationswolken versehen sind, den sogenannten *Triplonen*. Dieser effektive Hamiltonoperator beschreibt die Bewegung der Triplonen durch Hüpfamplituden, die als Polynome in der Kopplung x gegeben sind. Das Triplon ist ein Hardcore Boson, d.h. eine Spin 1 Anregung, wobei jeder Dimer auf der Leiter maximal mit einem Triplon besetzt werden kann.
Die bereits vorhandenen Ergebnisse der 1-Triplon und 2-Triplon Sektoren, auf denen diese Arbeit aufbaut, und die benutzten Methoden zur Berechnung der Spektraldichte werden dargestellt. In dieser Diplomarbeit wird die 3-Triplon Spektraldichte berechnet. Ein vereinfachtes Modell, in dem nur Wechselwirkungen berücksichtigt werden, ermöglicht bereits ein qualitatives Verständnis der Struktur des Anregungsspektrums der 3-Triplon Spektraldichte. Die 2-Teilchen und 3-Teilchen Spektraldichte und mögliche gebundene Zustände werden untersucht. Die Hardcore Eigenschaft ohne weitere Wechselwirkung der Teilchen untereinander unterdrückt die Bandkanten bereits signifikant. Für zwei freie Teilchen mit der gleichen Dispersion wie zwei einzelne Teilchen findet man eine $1/\sqrt{\omega}$ Singularität an den Bandkanten. Die Hardcore Eigenschaft der Teilchen führt im 2-Teilchen Sektor zu einem Wurzelverhalten $\sqrt{\omega}$ an den Bandkanten. Das allgemeine Bandkan-

tenverhalten, das man auf die Hardcore Wechselwirkung zurückführt, wird für das Nächst-Nachbar-Modell berechnet. Es ist für den n-Teilchen ($n > 1$) Sektor $\omega^{\frac{n^2-1}{2}}$. Dieses Verhalten wird durch die numerische Berechnung der Spektraldichte des Nächst-Nachbar-Modells in dem 2- und 3-Teilchen Sektor bestätigt. Hiermit lässt sich die Form der Bandkanten der Spektraldichte der Spin 1/2 Leiter erklären.
Das qualitative Verhalten der Spektraldichte im 3-Triplon Sektor wird durch die 1-Triplon und 2-Triplon Anteile des Hamiltonoperators bestimmt. Falls die untere Bandkante durch einen gebundenen Zustand von zwei Triplonen und einem ungebundenen Triplon gegeben ist, verhält sich die untere Bandkante nicht mehr kubisch in der Energie sondern besitzt dort einen Sprung. Die optische Leitfähigkeit beinhaltet einen magnetischen Beitrag, der durch die gleichzeitige Anregung von Triplonen und einem Phonon gegeben ist. In Holmpolarisation wird dieser Beitrag zur optischen Leitfähigkeit berechnet und es zeigt sich, dass der 3-Triplon Beitrag die Beschreibung der an $La_{5.2}Ca_{8.8}Cu_{24}O_{41}$ gemessenen optischen Leitfähigkeit verbessert. Um eine quantitativ bessere Beschreibung zu erlangen, sollte in Zukunft noch ein zusätzlicher Ringaustauschterm berücksichtigt werden, der dem 3-Triplonen Sektor eine stärkere Bedeutung geben wird. Die Ergebnisse renormalisierender Zugänge zur Gewinnung der Hüpfamplituden für größere Kopplungsstärken können übernommen werden, um mit den jetzt vorhandenen Programmen 3-Triplon Beiträge zur Spektraldichte zu berechnen.

Chapter 2

Introduction

Antiferromagnetic quantum spin systems are investigated intensively in theory and experiment [1]. In superconductors two electrons are bound together by an attractive force. In conventional superconductors this force is due to the electron-phonon interaction. A polarisation cloud of lattice distortions gives rise to bound states despite the strong Coulombic repulsion of two electrons. In copper-oxide-superconductors it is assumed that the attractive interaction is mediated by magnetic excitations [2]. The key structural unit is the CuO_2 plane so that the materials are quasi-two dimensional. Therefore low dimensional spin systems are the topic of vivid research activities in solid state physics.
The system considered in this thesis is the two-leg $S = \frac{1}{2}$ antiferromagnetic Heisenberg ladder at $T = 0$. Because quantum fluctuations are strong the classical Néel state is not the ground state [3]. Small spin and low dimensions favour a spin liquid state. The long-range order breaks down, but spins on neighbouring sites still tend to be antiparallel. If the distance of two spins in the ladder is large, a deviation from the Néel state becomes more probable. Spin waves are no more the elementary excitations. A natural choice for the elementary excitations is the triplon as will be explained below.
Spin liquids exhibit interesting physics: strongly interacting quasi-particles, bound states of quasi particles, quantum phase transitions and superconductivity under pressure upon hole doping to name a few [4]. An experimental realization of spin ladders can be found in compounds like $La_xCa_{14-x}Cu_{24}O_{41}$ [5] or $SrCu_2O_3$. In the former material spin chains are also present.

One- and two-triplon excitations has already been investigated before [27, 23, 24]. The next important contribution are the three-triplon excitations. It is assumed that including these corrections improve the consistency between theory and experiment, which will be checked in this work. The focus of this thesis lies on the investigation of the three-triplon spectral density for total spin 0, which is the quantity accessible by optical absorption experiments. The outline of this thesis is as follows:

- Chapter 2
  The quasi-particle, the *triplon*, is introduced and previous results for one and two triplons are presented.
- Chapter 3
  The evaluation of the spectral density is explained.
- Chapter 4
  A nearest neighbour hopping toy model is discussed for a qualitative understanding of the excitation spectra of two and three quasi-particles.
- Chapter 5
  The three-triplon spectral density of the Heisenberg ladder is presented and analyzed.

2.1 Quasi-Particle Picture: The Triplon

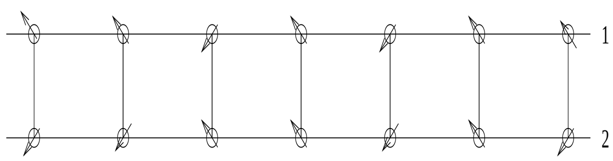

Figure 2.1: Two-leg spin ladder

The Hamiltonian of the two-leg ladder reads

$$H = \sum_i \left[J_\perp \mathbf{S}_{i,1}\mathbf{S}_{i,2} + J_{||}(\mathbf{S}_{i,1}\mathbf{S}_{i-1,1} + \mathbf{S}_{i,2}\mathbf{S}_{i-1,2})\right] \tag{2.1}$$

$$H/J_\perp = \sum_i \left[\mathbf{S}_{i,1}\mathbf{S}_{i,2} + x(\mathbf{S}_{i,1}\mathbf{S}_{i-1,1} + \mathbf{S}_{i,2}\mathbf{S}_{i-1,2})\right]. \tag{2.2}$$

Subscript i denotes the rungs with exchange coupling $J_\perp$ and $1,2$ refer to the two legs with coupling $J_{||}$ (see Fig. 2.1). The antiferromagnetism is expressed through positive values of the exchange couplings J. The total spin is conserved because the Hamiltonian is isotropic in the spin-coordinate space.
In this thesis the focus lies on the calculation of spectral densities. For a given observable $\mathcal{O}$ the $T = 0$K spectral density is given by the imaginary part of the Green's function

$$S(\omega) = -\frac{1}{\pi}\Im\langle 0|\mathcal{O}^\dagger(\omega - (H - E_0) + i0^+)^{-1}\mathcal{O}|0\rangle. \tag{2.3}$$

The energy E_0 is the ground state energy and the ground state is $|0\rangle$.

The calculation of $S(\omega)$ is a very complicated many-particle problem, but in the special case of $x = 0$ it can be solved by elementary quantum mechanics. In this case the system consists only of non-interacting dimers. Two coupled spins have four different states: three triplets ($|t_{-1}\rangle, |t_0\rangle, |t_1\rangle$) with total spin 1 and one singlet ground state $|s\rangle$ with total spin 0

$$
\begin{aligned}
|s\rangle &= \frac{1}{\sqrt{2}}(|\uparrow\downarrow\rangle - |\downarrow\uparrow\rangle) &\quad (2.4a)\\
|t^1\rangle &= |\uparrow\uparrow\rangle &\quad (2.4b)\\
|t^0\rangle &= \frac{1}{\sqrt{2}}(|\uparrow\downarrow\rangle + |\downarrow\uparrow\rangle) &\quad (2.4c)\\
|t^{-1}\rangle &= |\downarrow\downarrow\rangle. &\quad (2.4d)
\end{aligned}
$$

The main idea for the method employed is to develop a description of the full problem for small x starting from the isolated dimers. Therefore the problem is restated in the eigenbasis of the isolated dimers: singlets and triplets. Singlets have a lower energy than the triplets. The ladder is mapped onto a chain of singlets and triplets. The sites of the chain correspond to the rungs on the ladder (Figure 2.2). The eigenvalues of the rung Hamiltonian for the rung-singlet and the rung-triplet are

$$
\begin{aligned}
\mathbf{S}_1\mathbf{S}_2 &= \frac{1}{2}((\mathbf{S}_1+\mathbf{S}_2)^2 - \mathbf{S}_1^2 - \mathbf{S}_2^2) &\quad (2.5a)\\
\mathbf{S}_1\mathbf{S}_2|t\rangle &= \frac{1}{2}(1(1+1) - 2\frac{1}{2}(1+\frac{1}{2}))|t\rangle = \frac{1}{4}|t\rangle &\quad (2.5b)\\
\mathbf{S}_1\mathbf{S}_2|s\rangle &= \frac{1}{2}(0(0+1) - 2\frac{1}{2}(1+\frac{1}{2}))|s\rangle = -\frac{3}{4}|s\rangle. &\quad (2.5c)
\end{aligned}
$$

In this basis the Hamiltonian and the observables can be splitted in two

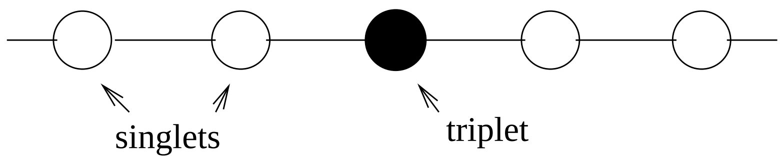

Figure 2.2: In the basis of singlets and triplets the ladder of spins becomes a chain of rungs.

parts 2.8): the triplets counting part Q and a perturbing part which can either destroy, create two triplets ($T_{\pm 2}$) or leave the number of triplets on adjacent dimers constant (T_0). The triplets counting part Q corresponds to the rung-coupling part; the perturbing part (T_n) to the leg-coupling part in the original Hamiltonian. The operator Q counts the number of rung-triplets present on the ladder. The T_n-operators consists of sums over all local operators τ_n (Table 2.1) which act locally on neighbouring rungs. They change the number of triplets by n.

$$\begin{aligned} T_n &= \sum_{\nu \in \text{adjacent rung dimers}} \tau_n(\nu) && (2.6) \\ [Q, T_n] &= nT_n && (2.7) \end{aligned}$$

	$2\tau_0$	
$\|t^{0,\pm1}, s\rangle$	$\longrightarrow$	$\|s, t^{0,\pm1}\rangle$
$\|t^0, t^{\pm1}\rangle$	$\longrightarrow$	$\|t^{\pm1}, t^0\rangle$
$\|t^{\pm1}, t^{\pm1}\rangle$	$\longrightarrow$	$\|t^{\pm1}, t^{\pm1}\rangle$
$\|t^{\pm1}, t^{\mp1}\rangle$	$\longrightarrow$	$\|t^0, t^0\rangle - \|t^{\pm1}, t^{\mp1}\rangle$
$\|t^0, t^0\rangle$	$\longrightarrow$	$\|t^1, t^{-1}\rangle + \|t^{-1}, t^1\rangle$
	$2\tau_2$	
$\|s, s\rangle$	$\longrightarrow$	$\|t^0, t^0\rangle - \|t^1, t^{-1}\rangle - \|t^{-1}, t^1\rangle$

Table 2.1: Action of the local operators τ_n acting on adjacent rungs. The superscript indicates the magnetic quantum number. The remaining matrix elements can be found by using $\tau_n^\dagger = \tau_{-n}$.

The Hamiltonian in the basis of triplets and singulets reads

$$H = Q + x(T_{-2} + T_0 + T_2). \tag{2.8}$$

It is possible to eliminate the operators which do not conserve the number of quasi-particles. This was done in Refs. [9, 12, 13, 14, 10, 11, 18] using the method of Continuous Unitary Transformations (CUT) introduced by F. Wegner [15].

2.1.1 Flow equation-Continuous Unitary Transformation

The basic idea is to transform the Hamiltonian and all observables in a continuous fashion. Therefore the flow parameter $l \in \mathbb{R}_0^+$ is introduced. $H(l = 0)$ is the original Hamiltonian and $H(l = \infty) = H_{\text{eff}}$ is the effective one which commutes with the quasi-particle counting operator Q. The evolution of the unitary transformation $U(l)$ is governed locally in l by the anti-hermitian generator $\eta(l) = -\eta^+(l)$.

$$\begin{aligned} H(l) &= U(l)H(0)U^+(l), && (2.9) \\ \frac{dU(l)}{dl} &= \eta(l)U(l) && (2.10) \end{aligned}$$

These two lines can be restated in the *flow equation*

$$\frac{dH(l)}{dl} = [\eta(l), H(l)], \tag{2.11}$$

$$\frac{d\mathcal{O}(l)}{dl} = [\eta(l), \mathcal{O}(l)]. \tag{2.12}$$

The observables have to be treated in the same way. So far the problem of finding a unitary transformation U has been restated in terms of the anti-hermitian generator η. If the generator is chosen as to be, e.g. the commutator of the triplet counting operator Q with H one can see that the variation of H with l vanishes if Q and H commute

$$\eta(l) = [Q, H(l)]. \tag{2.13}$$

This is the original generator proposed by Wegner, if Q is taken as the diagonal part [15].

In the limit of $l \to \infty$ a particle conserving Hamiltonian $H_{\text{eff}} = H(l = \infty)$ is reached. In this work a modified generator is employed, which conserves the blockbandstructure during the flow for intermediate values of l (see Fig. 2.3). This generator reads in the eigenbasis of Q as

$$\eta_{ij} = \text{sign}(q_i - q_j) h_{ij}. \tag{2.14}$$

For a detailed discussion on appropriate generators see Refs. [16, 10, 17].

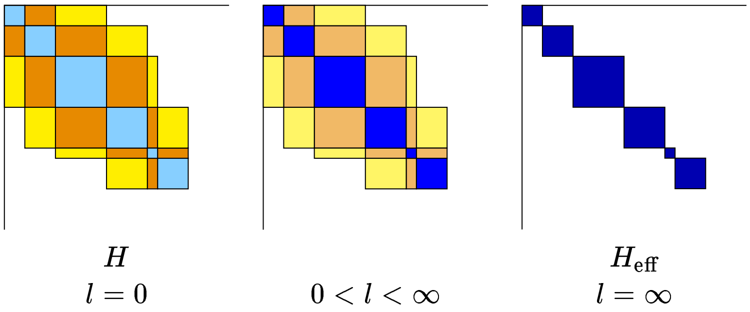

Figure 2.3: Illustration of the evolution of the Hamiltonian during the flow. For $l = 0$ the original Hamiltonian is depicted. During the flow the blockbandstructure is conserved due to the form of the generator 2.14. In the end an effective Hamiltonian H_{eff} is reached which conserves the number of particles $[Q, H_{\text{eff}}] = 0$. Only the blockdiagonal parts have non-zero values. Bright shading refers to small values and dark shading to bigger values in the Hamiltonian.

In general the Continuous Unitary Transformation is a non-perturbative method, if all terms generated by $[\eta, H]$ are kept.
However, certain truncations are necessary to make the problem tractable. One way is to expand all operators as series in a small parameter. One arrives at the following ansatz

$$\begin{aligned} H(x,l) &= Q + \sum_{k=1}^{\infty} x^k \sum_{\{m_1,..m_k\}} F(l;\{m_1..m_k\}) \prod_{i=1}^{k} T_{m_i} && \text{(2.15a)} \\ m_i &\in \{-2, 0, 2\}. && \text{(2.15b)} \end{aligned}$$

If inserted into the flow equation (2.11) then this gives a set of non-linear differential equations for the functions $F(l;\{m_1..m_k\})$. This ansatz includes all possible virtual excitation processes $\prod_{i=1}^{k} T_{m_i}$ in a given order k multiplied by the weight $F(l;\{m_1..m_k\})$. For $l=0$, the ansatz just reproduces the original Hamiltonian (2.8). The order k is the range of the local interaction in real space [18]. So the solution of the flow equation gives a perturbative series in the expansion parameter x up to some interaction range k. At $l=\infty$ only those terms remain which conserve the number of triplons:

$$H_{\text{eff}}(x) = Q + \sum_{k=1}^{\infty} x^k \sum_{\substack{\{m_1,..m_k\} \\ \sum_i m_i = 0}} C(\{m_1..m_k\}) \prod_{i=1}^{k} T_{m_i} \tag{2.16a}$$

$$m_i \in \{-2, 0, 2\}. \tag{2.16b}$$

The Hamiltonian is given as a polynomial in x. Each monomial $\prod_{i=1}^{k} T_{m_i}$ stands for a weighted quasi-particle conserving virtual process. The numbers $C(\{m_1..m_k\})$ are given by the solution of the flow equation as fractions of integers. They are the weight-factors for the virtual processes $T_{m_1}T_{m_2}..T_{m_k}$ in the given order k. These processes create the polarisation cloud of the dressed quasi- particle, the so called *triplon* [19]. They leave the number of particles in the system constant ($\sum_i m_i = 0$) since triplons are created only in intermediate states. The triplon is a triplet dressed with virtual excitation processes. It is a bosonic excitation with the restriction that a dimer can be excited only once. This justifies the term hardcore bosons for triplons. If a triplon is created through a local excitation process it can hop because of the inter-dimer coupling. Therefore the energy becomes k dependent. Two or more quasi-particles can interact, they have an excitation continuum and they can form bound states.

The order k determines the range of the polarisation cloud. By the linked-cluster theorem only connected virtual excitations have to be considered. The first order process T_0 can change the position of a triplon by one. A second order process like $T_{-2}T_2$ can lead to a hopping by two rungs. In general a kth order process can lead to a motion of an initial triplon by k rungs. So in the thermodynamic limit the Hamiltonian can be evaluated on finite clusters of size $k+1$. The number of virtual excitations becomes huge with growing k. In the one-/two- particle sector orders of $k=14$ and 13 were reached. The dimension of a Hilbert space of a cluster with 15 sites is $4^{15}=2^{30}$.

The effective Hamiltonian can now be examined in the different triplon sectors denoted by the lower index $|_n$ where n describes the number of triplons present

$$H_{\text{eff}}|_n = H_0|_n + H_1|_n + H_2|_n + \cdots H_n|_n. \tag{2.17}$$

For instance $H_1|_2$ describes the independent motion of two triplons. The

only interaction is due to the hardcore constraint that they cannot occupy the same site.
Clearly, there is no possibility for an irreducible five particle interaction in the three particle sector so that all terms like $H_m|_n$with $m > n$ vanish. Although H_n is defined on the entire Hilbert space it is sufficient to know H_n in the n-particle Hilbert space. Therefore a recursion scheme can be set up to extract the one, two and three particle irreducible (inter-)action [11]

$$
\begin{aligned}
H_0|_0 &= H_{\text{eff}}|_0 && \text{(2.18a)}\\
H_1|_1 &= H_{\text{eff}}|_1 - H_0|_1 && \text{(2.18b)}\\
H_2|_2 &= H_{\text{eff}}|_2 - H_0|_2 - H_1|_2 && \text{(2.18c)}\\
H_3|_3 &= H_{\text{eff}}|_3 - H_0|_3 - H_1|_3 - H_2|_3. && \text{(2.18d)}
\end{aligned}
$$

The first step is to know the ground state energy E_0 which defines H_0. The next step is to describe the dynamics of a single particle correctly. The irreducible two particle interaction is obtained if the processes which can be described as a motion of one particle are subtracted. True three particle interactions are described by H_3. From now on the subscript 'eff' is omitted. Every Hamiltonian is understood to be the particle conserving effective one. The plain series can be trusted up to $x \approx 0.5 - 0.6$. Standard Dlog-Padé- or Padè-extrapolations give reliable and stable approximations even for $x >$ 0.5. Figure 2.4 [18] shows that the extrapolation of the plain series is well defined. The gap $\Delta(x)$ can be extrapolated reliably up to $x \approx 2$ using Dlog Padé-approximations [21]. For $x \to \infty$ –the isolated chain limit- the gap closes and a phase transition occurs. So the gap is a measure for the distance to the phase transition. It is expected that the series becomes much simpler, i.e. much less singular, if we rewrite the expansion in the quantity $G(x)$ instead of x [20]

$$G(x) = 1 - \hat{\Delta}(x). \tag{2.19}$$

The rescaled gap is $\hat{\Delta}(x) = \frac{\Delta}{J_\perp + J_\parallel}$. It is one for $x = 0$, and zero for $x \to \infty$. The natural internal energy scale $G(x)$ grows from zero to one for x increasing from zero to one. So $G(x)$ is a more physical expansion parameter. The Gap equation can be inverted and gives than an expression for $x(G)$. The Padé-approximation after expressing x by G gives better results.

2.2 One-particle sector

The possible spin states in the one particle sector are $|t^{-1}\rangle, |t^0\rangle, |t^1\rangle$. The ladder or the chain (see Fig. 2.2) are translationaly invariant. In order to exploit this invariance a momentum basis is introduced. The state where one triplon is located at the site r on the chain while all other sites of the chain are in the singlet ground state is denoted by $|r\rangle$. For simplicity of the

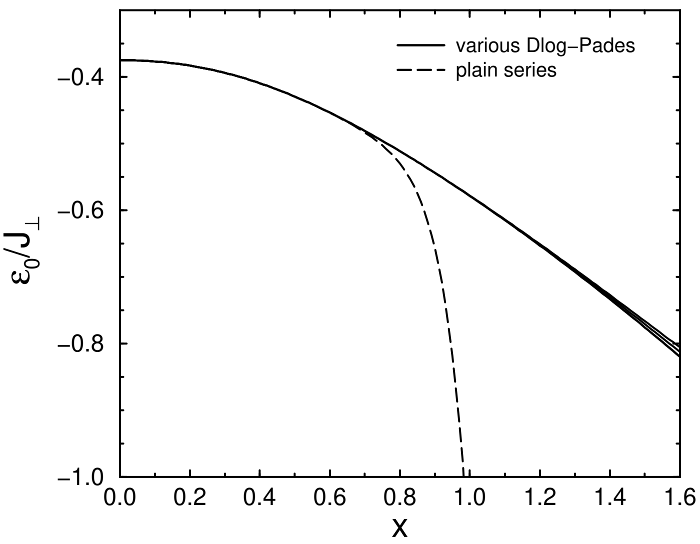

Figure 2.4: Ground state energy per spin as function of x. The plain series result is depicted as the dashed line. Four different Dlog-Padé-approximations are shown as solid lines. The extrapolation is stable and can be trusted even for $x > 1$.

notation I will focus on the position of the triplon in the next few lines only. The momentum state is given as

$$|K\rangle = \frac{1}{\sqrt{N}} \sum_r \exp(iKr)|r\rangle. \tag{2.20}$$

Calculation of the action of the Hamiltonian yields

$$\begin{aligned} H_{\text{eff}}|r\rangle &= (Q + H_0|_1 + H_1|_1)|r\rangle & (2.21)\\ &= (1 + E_0)|r\rangle + \sum_d t_d|r + d\rangle & (2.22) \end{aligned}$$

where E_0, t_d are polynomials in x. The inversion symmetry for the system gives $t_d = t_{-d}$, and translational symmetry justifies that one index d for the thermodynamic one-triplon hopping amplitudes is enough to define the hopping unambiguously.
The action of H on the momentum state gives the dispersion and shows that

the one triplon sector is diagonal in momentum space.

$$
\begin{aligned}
H_1|K\rangle &= \frac{1}{\sqrt{N}}\sum_{r,d}\exp(iKr)t_d|r+d\rangle && \text{(2.23a)}\\
&= \frac{1}{\sqrt{N}}\sum_{r,d}\exp(iK(r-d))t_d|r\rangle && \text{(2.23b)}\\
&= \sum_{d}\exp(iK(r-d))t_d\underbrace{\frac{1}{\sqrt{N}}\sum_{r}\exp(iKr)|r\rangle}_{|K\rangle} && \text{(2.23c)}\\
&= \left(t_0+2\sum_{d>0}t_d\cos(dk)\right)|K\rangle && \text{(2.23d)}\\
\Rightarrow H_{\text{eff}}|K\rangle &= \left(E_0+\underbrace{1+t_0+2\sum_{d>0}t_d\cos(dk)}_{\omega(K)}\right)|K\rangle && \text{(2.23e)}
\end{aligned}
$$

For finite gap the coefficients $t_d(x)$ decrease fast with increasing d. If the value of x is increased, the one-particle hopping range becomes larger but is still of finite range for $x \leq 1$ ($|t_{14}| < 0.0002|t_0|$ for $x \leq 1$). The dispersion $\omega(K)$ is the K dependent excitation energy of one triplon (see Fig. 2.5)

$$\omega(K) = \langle K|H_{\text{eff}}|_1 - H_0|_1|K\rangle. \tag{2.24}$$

For $x = 0$ there is no K dependence of the energy. The excitation energy is unity for all wave numbers. For small x the dispersion $\omega(K)$ is mainly cosine-like but it develops an additional dip at $K = 0$ with increasing x. The gap Δ can be read off at $K/\pi = 1$ (see fig. 2.5) .

2.3 Two-particle sector

Neglecting the actual position of the triplons and focusing on the spin space, two triplons with spin 1 can couple to total spin $S = \{0, 1, 2\}$ with magnetic quantum numbers m (See Table 2.2). The Hamiltonian is isotropic in spin space so the total spin and the magnetic quantum numbers are conserved.

Translational invariance of the ladder implies that the total momentum is conserved. In the position space of two triplons it is convenient to work with the relative distance. The relative momentum in the center of mass system is not conserved. Therefore the relative distance d generically leads to the formation of a two-particle continuum. These arguments are also true for higher n-particle sectors where the Fourier transforms of all $d_1, ..d_{n-1}$

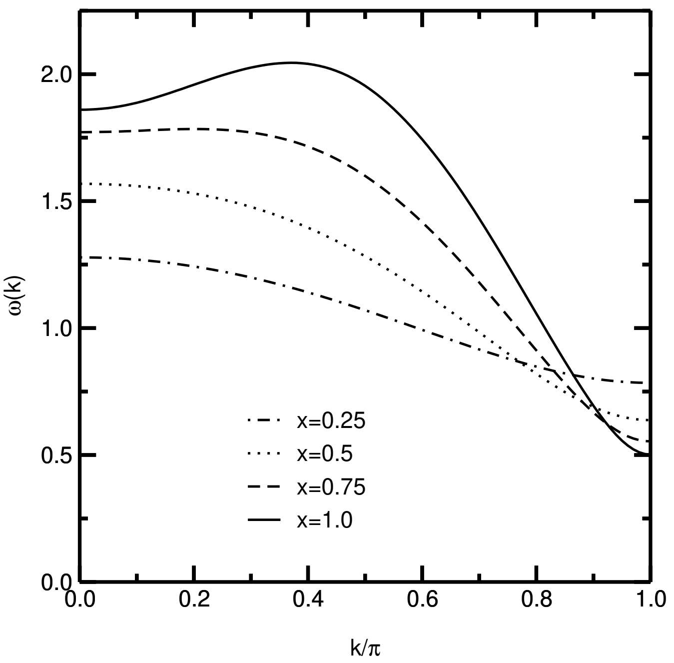

Figure 2.5: Dispersion $\omega(k)$ for various couplings x. See also Ref. [18].

relative distances is not a diagonal eigenbasis for the Hamiltonian. The one-particle sector gives the dispersion, higher particle sectors give continua.
The state $|r, r+d\rangle$ specifies one triplon at position r and the other at position $r+d$. The particles are indistinguishable. It cannot be said that particle one is left to particle two. For this reason an overcomplete basis has to be avoided. One possible solution is to restrict the relative distance d to positive values. So the first position always has to be smaller than the right position in the ket.

The action of H_1 shifts only one triplon at a time with the amplitudes $t_{d'}$ from the previous section

$$H_1|r, r+d\rangle = \sum_{d'} \left(|r+d', r+d\rangle + |r, r+d+d'\rangle\right) . \qquad (2.25)$$

If two triplons are present there are processes possible which violate the notation convention, i.e. they change the order in the notation if $r+d' > r+d$ or $r > r+d+d'$. So the two particles have to be exchanged. The total spin S is conserved and determines the exchange parity

$$\begin{aligned} P|r+d, r\rangle|S, m\rangle &= |r, r+d\rangle P|S, m\rangle & (2.26)\\ &= (-1)^S|r, r+d\rangle|S, m\rangle. & (2.27)\end{aligned}$$

The operator P exchanges the two particles in real space and spin space. For the action in spin space see Table 2.2. The two-triplon momentum state

S	m	
2	2	$\|t^1, t^1\rangle$
2	1	$\frac{1}{\sqrt{2}}(\|t^0, t^1\rangle + \|t^1, t^0\rangle)$
2	0	$\frac{1}{\sqrt{6}}(\|t^{-1}, t^1\rangle + 2\|t^0, t^0\rangle + \|t^1, t^{-1}\rangle$
2	-1	$\frac{1}{\sqrt{2}}(\|t^0, t^{-1}\rangle + \|t^{-1}, t^0\rangle)$
2	-2	$\|t^{-1}, t^{-1}\rangle$
1	1	$\frac{1}{\sqrt{2}}(\|t^1, t^0\rangle - \|t^0, t^1\rangle$
1	0	$\frac{1}{\sqrt{2}}(\|t^1, t^{-1}\rangle - \|t^{-1}, t^1\rangle$
1	-1	$\frac{1}{\sqrt{2}}(\|t^0, t^{-1}\rangle - \|t^{-1}, t^0\rangle$
0	0	$\frac{1}{\sqrt{3}}(\|t^0, t^0\rangle - \|t^1, t^{-1}\rangle - \|t^{-1}, t^1\rangle$

Table 2.2: The possible couplings of two spin 1 particles. S is the total spin, m the magnetic quantum number.

is defined up to an arbitrary phase by

$$|K, d\rangle|S, m\rangle = \frac{1}{\sqrt{N}} \sum_r \exp(i(r + d/2))|r, r + d\rangle|S, m\rangle. \tag{2.28}$$

The exchange reads in momentum space $|K, -d\rangle = (-1)^S|K, d\rangle$. The calculation of H_1 is more involved than in the one triplon sector. The result [18] is

$$H_1|K, d\rangle|S, m\rangle = 2\sum_{d' \neq d} t_{d'} \cos(Kd'/2)(\text{sign}(d - d'))^S|K, |d - d'|\rangle|S, m\rangle. \tag{2.29}$$

In this basis $H_1|_2$ is not diagonal. The sign function is understood to vanish for vanishing argument. For all distances d there is an action of H_1 which changes the relative distance up to 14 sites in order 14.

The operator H_2 may move both particles at the same time. Two initial and two final positions make it possible to label the processes uniquely. The translational invariance of the ladder allows to specify just the relative movements and distances: d-the initial relative distance, r'-the shift oft the left triplon and d' the final relative distance (see Fig. 2.6)

$$H_2|r, r + d\rangle|S, m\rangle = \sum_{r', d'} t^S_{d,r',d'}|r + r', r + r' + d'\rangle|S, m\rangle. \tag{2.30}$$

The translational invariance and inversion symmetry of the ladder is reflected in the hopping amplitudes by

$$t_{d,r',d'} = t_{d,-r'-d'+d,d'}. \tag{2.31}$$

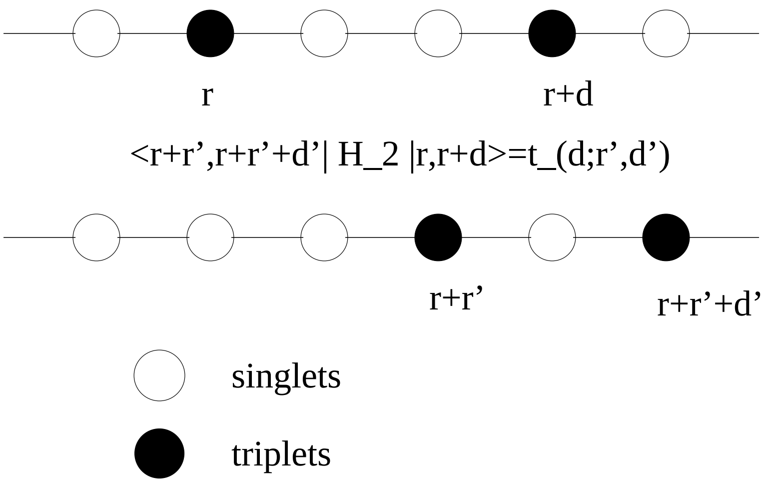

Figure 2.6: Illustration of the action of H_2. The hopping is due to the translational symmetry of the ladder independent of the absolute position r.

They are polynomials in x like all other amplitudes. This relation is used to calculate [16]

$$
\begin{aligned}
H_2|K,d\rangle|S,m\rangle = \Bigg(& \sum_{d'} t_{d,(d-d')/2,d'} + \\
& 2\sum_{r'>(d-d')/2,d'} t_{d,r',d'} \cos(K(r'-\frac{d-d'}{2}))\Bigg) |K,d'\rangle|S,m\rangle
\end{aligned} \quad . \tag{2.32}
$$

The sums run over $d', r' \in \mathbb{Z}$. $t_{d,(d-d')/2,d'}$ is only different from zero if $(d-d')/2 \in \mathbb{Z}$. Only at small distances H_2 contributes. At large distances the two triplon dynamics are solely governed by the independent one-triplon hopping. The action of H_2 can give rise to two bound states (S=0, S=1) below the 2-triplon continuum (see Figs. 2.7,2.8).

Figures 2.7, 2.8 give an overview over the energies of the two-,three- and four triplon band edges of the spectral densities [22]. In Chapter 4 the three triplon sector is discussed. The two-triplon sector was investigated before by K.P. Schmidt, K. Knetter and G.S. Uhrig.

2.4 Observables

States with total spin 1 can be observed by neutron scattering. By Raman scattering states with total spin 0 are excited. Conventional Raman experiments are restricted to $K = 0$. Infrared spectroscopy with an excitation

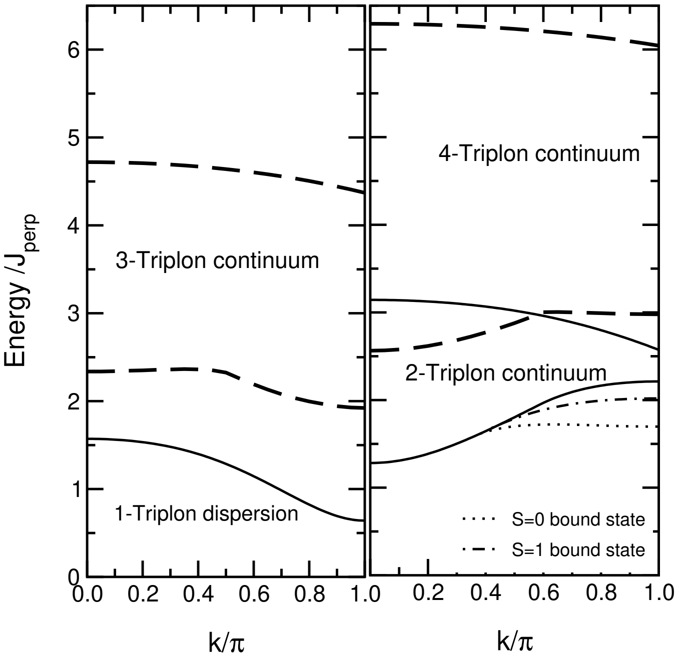

Figure 2.7: Dispersion and band edges of the spectral densities for $x = 0.5$ [22]. The continua overlap. The dispersion and the two-triplon contribution were calculated before [23].

of a phonon at the same time makes it possible to observe also $S = 0$ excitations with arbitrary momentum [25, 26]. The phonon is needed for the momentum transfer. The inversion symmetry between neighbouring spins is also broken by the phonon. The presence of a center of inversion inhibits any asymmetric displacement of charge and hence the associated dipole moment vanishes. The observables for magnetic light scattering in rung-rung (leg-leg) polarization are in leading order proportional to the superposition of rung (leg) coupling part of the Hamiltonian [6, 7, 8].

$$\mathcal{O}^{\text{rung}} = A^{\text{rung}}\mathbf{S}_{i,1}\mathbf{S}_{i,2} \tag{2.33}$$

$$\begin{aligned}
\mathcal{O}^{\text{leg}} &= A^{\text{leg}}\mathbf{S}_{i,1}\mathbf{S}_{i-1,1} && \text{(2.34a)}\\
&= \frac{A^{\text{leg}}}{2}(\mathbf{S}_{i,1}\mathbf{S}_{i-1,1} - \mathbf{S}_{i,2}\mathbf{S}_{i-1,2}) && \text{(2.34b)}\\
&\quad +\frac{A^{\text{leg}}}{2}(\mathbf{S}_{i,1}\mathbf{S}_{i-1,1} + \mathbf{S}_{i,2}\mathbf{S}_{i-1,2}) && \text{(2.34c)}
\end{aligned}$$

The factors $A^{\text{leg}}, A^{\text{rung}}$ depend on the underlying microscopic model.
The ladder is symmetric under exchange of the two legs. Let $\mathcal{P}$ be the

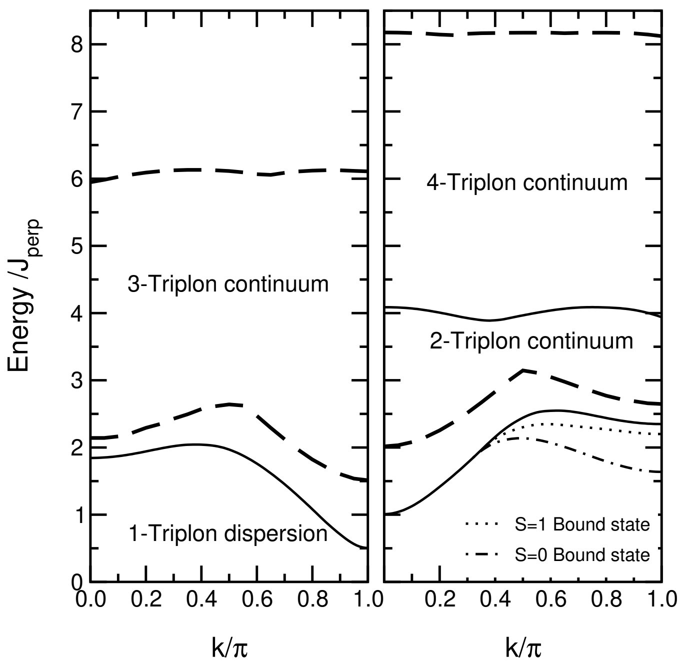

Figure 2.8: Band edges of the spectral densities for $x = 1.0$ [22]. The overlap of the two-, three- and four-triplon sectors becomes larger as compared to the sectors for $x = 0.5$ (See Fig. 2.7) because the continua are broader in energy. So for the coupling $x = 1$ the three-/four-triplon sector can contribute at lower energies as compared to $x = 0.5$.

operator which interchanges the two legs. A single rung-singlet (-triplon) has odd (even) parity with respect to $\mathcal{P}$. The state with singlets on all rungs is defined to be of even parity $\mathcal{P}|0\rangle = |0\rangle$. The relative parity of the excitation, the triplon, is odd. Therefore, if $|n\rangle$ denotes a state with n singlets excited to triplons then $\mathcal{P}|n\rangle = (-1)^n|n\rangle$. The CUT does not change the parities because the generator commutes with the parity operator $[\eta, \mathcal{P}] = 0$. The generator consists of sums over products of creation and annihilation operators T_{-2}, T_2, T_0. Each of them commutes with the parity operator. Therefore an even (odd) observable $\mathcal{O}$ can excite only an even (odd) number of triplons. The rung polarisation operator $\mathcal{O}^{\text{rung}}$ (2.33) has even parity. Some operators like $\mathcal{O}^{\text{leg}}$ (2.34a) have even (2.34c) and odd (2.34b) contributions.

Here it is interesting to look at the spectral weights of the observables $I_{tot} = I_0 + I_1 + I_2 + I_3 + .. + I_n$ contained in the $n-$triplon sector. The spectral weight in each of these subspaces is defined by

$$I_n = \langle 0|\mathcal{O}^\dagger P_n \mathcal{O}|0\rangle \tag{2.35}$$

where P_n projects onto the subspace with $n-$triplons. This definition is reasonable only because of the particle conserving property of the Hamiltonian after the transformation. Figure 2.9 shows that the one-triplon sector is

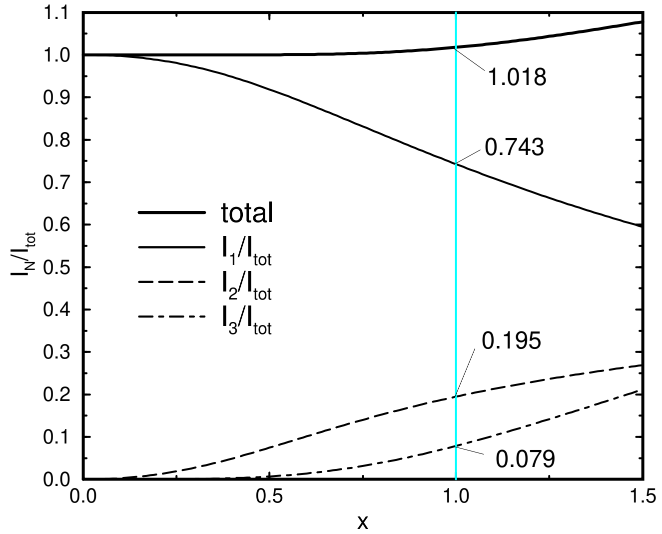

Figure 2.9: Relative weights for the $S = 1$ operator $\mathbf{S}^z_{1,i}$ in the n-triplon sectors and the total intensity.

the dominant contribution to the $S = 1$ operator $S^z_{1,i}$. The two- and three-triplon contributions are the next largest. In Fig. 2.10 it can be seen that the triplon is a good choice for the quasi-particle in the ladder system. For x not too large most of the spectral weight is captured by a few triplons [27, 23, 24]. The three triplon sector, which is examined in this thesis, is the next important contribution after the two-triplon sector which was already investigated before. Compared to the $S = 1$ operator (see Fig. 2.9) the three-triplon sector is more important for the $S = 0$ operator. For $x = 0$ the singlet made from two isolated-rung triplons contains the full weight of the considered operator. Two triplons are needed to couple to total spin $S = 0$.

Measurements were performed on $La_{5.2}Ca_{8.8}Cu_{24}O_{41}$. For an infrared experiment, where a phonon is excited at the same time, only momentum space integrated intensities are observable. The dispersion of the phonon is of minor importance, so it is assumed to be an Einstein-phonon with constant energy ω_{Ph}. For the leg- (2.34a) and the rung-operator (2.33) the involved phonons are different ($\omega^{leg}_{\mathrm{Ph}} = 570\mathrm{cm}^{-1}$, $\omega^{rung}_{\mathrm{Ph}} = 620\mathrm{cm}^{-1}$). For this material the rung-exchange coupling is $J_\perp \approx 1000\mathrm{cm}^{-1}$ and the rung-rung

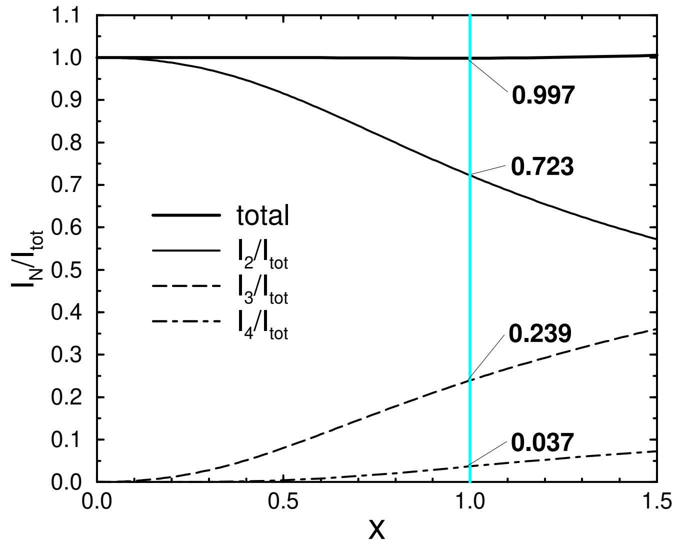

Figure 2.10: Relative weights for the $S = 0$ operator $\mathbf{S}_{1,i}\mathbf{S}_{1,i+1}$

.

coupling $x = J_{||}/J_{\perp} \approx 1.0 - 1.3$. The optical conductivity is a weighted superposition of the momentum resolved spectral density

$$\sigma(\omega - \omega_{Ph}) = \omega \int dk f^2(k) S(k, \omega). \tag{2.36}$$

The form factor $f(k)$ in leading order reads [25, 28, 5] $f(k) \propto \sin^4(k/2)$. The optical conductivity is dominated by its contribution at higher momenta close to the Brillouin boundary.

The optical conductivity connects the spectral density to an experimentally accessible observable. In Fig. 2.11 the calculated two-triplon contribution is compared to the experimental data. In this calculation an additional four-spin correction, the cyclic-exchange, was also incorporated in the Hamiltonian. Qualitatively, the spectra agree very well with each other. In the polarisation parallel to the leg (top panel) there is the largest discrepancy between 3000cm^{-1} and 5500cm^{-1}. In this thesis it will be shown how much the three-triplon contribution will improve the agreement.
For the rung-polarisation only contributions with an even number of triplons are allowed. The bandwidth in this case is underestimated by the perturbative CUT method.

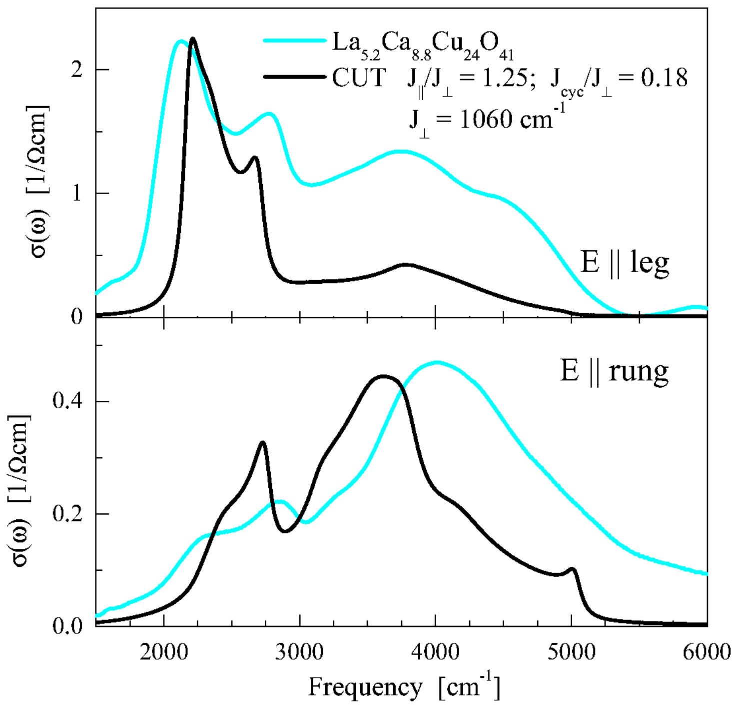

Figure 2.11: Comparison of $\sigma(\omega)$ of $La_{5.2}Ca_{8.8}Cu_{24}O_41$ (gray lines) at $T =$ 4K with the two-triplon contribution calculated by CUT (black lines) for $x =$ 1.25, $J_{cycl}/J_{\perp} = 0.18$, $J_{\perp} = 1000\text{cm}^{-1}$,$\omega_{\text{Ph}}^{leg} = 570\text{cm}^{-1}$, $\omega_{\text{Ph}}^{rung} = 620\text{cm}^{-1}$ and a finite broadening $\delta = 0.02J_{\perp}$. (**Top panel**) Polarisation parallel to the legs. The three-triplon part is missing.(**Bottom panel**) Polarisation parallel to the rungs. The missing four-triplon part is of minor importance (see Fig. 2.10). This figure is taken from Ref. [5].

Chapter 3

Spectral Densities

The spectral density contains information about the excitations of the system (H) and about the way the system is experimentally excited ($\mathcal{O}$). For $T = 0$ it reads

$$S(\boldsymbol{K}, \omega) = \langle 0|\mathcal{O}^+(\boldsymbol{K})\delta(\omega - (H(\boldsymbol{K}) - E_0))\mathcal{O}(\boldsymbol{K})|0\rangle. \tag{3.1}$$

The energy and momentum resolved spectral density $S(\boldsymbol{K}, \omega)$ is calculated using the retarded zero temperature Green's function $G(\boldsymbol{K}, \omega)$

$$\begin{aligned} G(\boldsymbol{K}, \omega) &= \langle 0|\mathcal{O}^+(\boldsymbol{K})\frac{1}{\omega - (H(\boldsymbol{K}) - E_0) + i\eta}\mathcal{O}(\boldsymbol{K})|0\rangle & (3.2) \\ &= \mathcal{P}\langle 0|\mathcal{O}^+(\boldsymbol{K})\frac{1}{\omega - (H(\boldsymbol{K}) - E_0)}\mathcal{O}(\boldsymbol{K})|0\rangle \\ &\quad -i\pi\langle 0|\mathcal{O}^+(\boldsymbol{K})\delta(\omega - (H(\boldsymbol{K}) - E_0))\mathcal{O}(\boldsymbol{K})|0\rangle. & (3.3) \end{aligned}$$

Dirac's identity is used in the last line

$$\frac{1}{x - x_0 \pm i0^+} = \mathcal{P}\frac{1}{x - x_0} \mp i\pi\delta(x - x_0). \tag{3.4}$$

$\mathcal{P}$ denotes Cauchy's principal value. The spectral density can be read off

$$S(\boldsymbol{K}, \omega) = -\frac{1}{\pi}\Im G(\boldsymbol{K}, \omega). \tag{3.5}$$

In most cases a simple analytic expression cannot be given for the Green's function. If this is the case the Hamiltonian can be tridiagonalized, which allows an easy evaluation of the Green's function in a continued fraction. An important point is that the calculation of the Green's function does not involve the calculation of the eigenstates and eigenvectors of the Hamiltonian. Less is needed to extract the physical properties of interest here. The local physics (no long range order) of a local excitation ($\mathcal{O}|0\rangle$) is governed by its environment. The tridiagonalization is done by the Lanczos-algorithm.

3.1 Tridiagonalisation or Lanczos-algorithm

Given an initial state $|q_1\rangle = \mathcal{O}|0\rangle$ and the Hamiltonian H, the idea is to build an orthonormal Krylov sequence $(|q\rangle, H|q\rangle, H^2|q\rangle, H^3|q\rangle, ...)$. The new orthonormal basis $\{|q_i\rangle\}$ of the Krylov sequence is constructed via the following recursion scheme [30]

$$\begin{aligned} |q_1\rangle &= \mathcal{O}|0\rangle && (3.6) \\ H|q_i\rangle &= b_i|q_{i-1}\rangle + a_i|q_i\rangle + b_{i+1}|q_{i+1}\rangle \text{ for } i \geq 1. && (3.7) \end{aligned}$$

Terms with non positive indices are set to zero. The recursion is essentially a $H^n\mathcal{O}|0\rangle$ expansion with additional Gram-Schmidt-orthogonaliziation to the previous constructed states. The a_i coefficients are real, because the Hamiltonian is hermitian and $b_i \geq 0$, because the norm is always non-negative:

$$\begin{aligned} a_i &= \langle q_i|H|q_i\rangle && (3.8a) \\ b_{i+1} &= \sqrt{\langle r_i|r_i\rangle} \text{ with } |r_i\rangle = H|q_i\rangle - a_i|q_i\rangle - b_i|q_{i-1}\rangle && (3.8b) \\ |q_{i+1}\rangle &= \frac{|r_i\rangle}{b_{i+1}} \text{ if } b_{i+1} \neq 0. && (3.8c) \end{aligned}$$

The matrix representation H_{Tri} of H in this new basis is tridiagonal. The transformation $Q[q_1, q_2, q_3, ..]$ consists of orthonormal rows, i.e.

$$Q^+HQ = H_{\text{Tri}} \text{ with } Q^+Q = 1. \tag{3.9}$$

Hence H_{Tri} has the same eigenvalues as H. In this basis the Hamiltonian is tridiagonal

$$(\omega - H_{\text{Tri}}) = \begin{pmatrix} \omega - a_1 & -b_2 & 0 & \cdots \\ -b_2 & \omega - a_2 & -b_3 & \ddots \\ 0 & -b_3 & \ddots & \ddots \\ \vdots & \ddots & \ddots & \end{pmatrix}. \tag{3.10}$$

To evaluate the Green's function not the full inverse of $(\omega - H)$ has to be computed, but the entry $\langle q_1|(\omega - H)^{-1}|q_1\rangle$. Let D_n denote the matrix $\omega - H_{\text{Tri}}$ where the first n rows and columns are removed. Because of the simple structure of H_{Tri} an easy recursion scheme is found for the determinant by using Cramer's rule

$$\det(D_n) = (\omega - a_{n+1})\det(D_{n+1}) - b_{n+2}^2\det(D_{n+2}) \tag{3.11}$$

So the desired matrix element becomes

$$\langle q_1|(\omega - H_{Tr})^{-1}|q_1\rangle = \langle q_1|q_1\rangle \frac{\det(D_1)}{\det(D_0)} \tag{3.12a}$$

$$= \frac{\langle q_1|q_1\rangle}{(\omega - a_1) - b_2^2 \det(D_2)/\det(D_1)} \tag{3.12b}$$

$$= \frac{\langle q_1|q_1\rangle}{\omega - a_1 - b_2^2 \dfrac{1}{\omega - a_2 - b_3^2 \dfrac{1}{\omega - a_3 - \ldots}}}. \tag{3.12c}$$

The tridiagonalization was implemented using a computer system.

The infinite Hilbert space is approximated by a finite set of basis vectors, e.g. the relative distances between the particles are restricted to a maximum value. Each application of the Hamiltonian corresponds to further enlarging of the range of the initial excitation. So with each recursion step more possible paths of the initial excitation are taken into account [29].

For three particles the upper limit for the relative distance of triplons lies between $200 - 300$ to remain within a reasonable computation time. Otherwise the computation time becomes too large. The interactions are relatively local in real space so triplons with relative distance greater than the range of interaction act as free triplons. So even with much fewer sites than the possible $200 - 300$ the approximation becomes stable and the spectral density does not change by extending the basis anymore.

The finite Hilbert space of restricted relative triplon distances for the ladder is large but the Hamiltonian is sparse and block diagonal. For such matrices the tridiagonalization scheme is fast. Each application of the Hamiltonian costs little time. The Hamiltonian has not to be stored as a matrix, but can be implemented as a case differentiation.

Due to rounding errors the new basis vectors can loose their orthonormality. So the vectors were additionally orthonormalized to all previous ones in each recursion step.

3.2 Asymptotic Behaviour of Continued Fraction Coefficients

The dimension of the spin ladder Hilbert space is infinite. So in principal the infinite numbers of constants a_i, b_i with $i \in \mathbb{N}$ have to be known to calculate the analytical exact Green's function. Only in a few special cases all these numbers can be given directly without evaluating the recursion step by step. Because of the limitation of computational time and space the recursion has to be stopped after N_0 iterations. In this work the focus lies on systems with finite support of the spectral density. This has the effect that the coefficients converge towards limits a, b after a few iterations. These limits are related to the center (a) and to the width (b) of the spectral density as will be explained below.

3.2.1 Termination of the continued fraction

One possibility to deal with the finite series of recursion coefficients is to leave the series incomplete and to introduce a finite small broadening η

$$\omega \to \omega + i\eta. \tag{3.13}$$

The Green's function has poles at the eigen energies, i.e. the denominator becomes zero. The slight broadening will smear out all poles to give a smooth function. This already resolves the structure of the spectral density accessible by an experimental setup. In an experiment the structures are also broadened due to finite life time effects which occur because the measurement are performed at finite temperature.
A better resolution of the spectral density is obtained by the proper termination of the continued fraction. With each application of the Hamiltonian the triplons become more wide spread over the ladder compared to the initial positions. So interaction effects between them become small. With increasing number of Lanczos-steps the action of H becomes more and more like H_1 where the hardcore constraint is also of minor importance due to the large relative average distances. So the band edges E_{max}, E_{min} can be calculated using the sum of the dispersions of free triplons and possible bound states. For two triplons this means:

$$E_{\max}(K) = \max((\omega(q_1) + \omega(q_2))|_{q_1+q_2 \equiv K} \tag{3.14}$$
$$E_{\min}(K) = \min((\omega(q_1) + \omega(q_2))|_{q_1+q_2 \equiv K}). \tag{3.15}$$

As one can see below (see Fig. 3.1), the band edges are related to the limits a, b [31] by

$$b = \frac{E_{\max} - E_{\min}}{4} \tag{3.16}$$
$$a = \frac{E_{\max} + E_{\min}}{2}. \tag{3.17}$$

So the finite series of a_i, b_i can be completed by a terminator which corresponds to appending an infinite series of constant a and b in the continued fraction. If $a_i = a$ and $b_i = b \quad \forall i \in \mathbb{N}$ the recursion can be solved by an exact expression for the terminator τ

$$\tau = \frac{1}{\omega - a - b^2\tau} \tag{3.18}$$

$$\Rightarrow \tau = \begin{cases} \frac{1}{2b^2}\left(\omega - a \pm \sqrt{(\omega - a)^2 - 4b^2}\right) & \text{for } (\omega - a)^2 \geq 4b^2 \\ \frac{1}{2b^2}\left(\omega - a \pm i\sqrt{4b^2 - (\omega - a)^2}\right) & \text{for } 4b^2 \geq (\omega - a)^2 \end{cases} \tag{3.19}$$

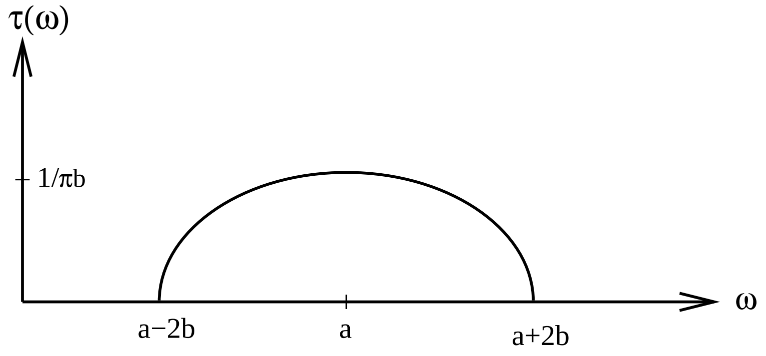

Figure 3.1: Elliptic spectral density for the square root terminator.

The signs have to be chosen such that the weight function is positive and that the Green's function has the right asymptotic behaviour ($\lim_{\omega\to\infty} = \frac{1}{\omega-\omega_B}$ where ω_B is an eigenenergy)

$$\Rightarrow \tau = \begin{cases} \frac{1}{2b^2}\left(\omega - a + \sqrt{(\omega-a)^2 - 4b^2}\right) & \text{for } \omega - a \leq -|2b| \\ \frac{1}{2b^2}\left(\omega - a - i\sqrt{4b^2 - (\omega-a)^2}\right) & \text{for } 4b^2 \geq (\omega-a)^2 \\ \frac{1}{2b^2}\left(\omega - a - \sqrt{(\omega-a)^2 - 4b^2}\right) & \text{for } \omega - a \geq |2b|. \end{cases} \tag{3.20}$$

So the spectral density of a continued fraction with constant coefficients is a symmetric half ellipse with center a, width $4b$ and height $\frac{1}{\pi b}$ (see Fig. 3.1)

$$S_\tau(\omega) = -\frac{1}{\pi}\Im\tau \tag{3.21}$$

$$= \frac{1}{2\pi b^2}\sqrt{4b^2 - (\omega-a)^2}. \tag{3.22}$$

The band edges are $\{a-2b, a+2b\}$. This square root terminator corresponds to a free next neighbour hopping model of two hardcore bosons (for further details see chapter 4). This is also equivalent to a boson hopping to the right nearest site on a semi-infinite chain starting on site $i = 0$.

3.3 Behaviour of $S(\omega)$ at the band edges

For various spectral densities the asymptotic behaviour of the recursion coefficients a_i, b_i is known, i.e. how the limits a, b are approached [31]. For a density of states of the form

$$S(\omega) = c(a + 2b - \omega)^\alpha (a - 2b + \omega)^\beta \text{ for } a - 2b \leq \omega \leq a + 2b \tag{3.23}$$

the asymptotic behaviour is

$$a_n - a = b\frac{\beta^2 - \alpha^2}{2n^2} + O(n^{-3}) \tag{3.24a}$$

$$b_n - b = b\frac{1 - 2\alpha^2 - 2\beta^2}{8n^2} + O(n^{-3}). \tag{3.24b}$$

If the band edges are known the exponents α, β can be extracted from the series a_n, b_n up to the signs.

3.3.1 Internal Singularities

Not only the behaviour of the spectral density at the band edges can give a contribution to the asymptotics of the recursion coefficient series but also internal singularities. There are also some relations derived which are useful in the analysis of the spectral density. For the singularities it is more convenient to work with a single reduced perturbation α_n, rather than the pair of recursion coefficients (a_n, b_n)

$$\alpha_{2n} = \frac{a_{n-1} - a}{b} \tag{3.25a}$$

$$\alpha_{2n+1} = 2\frac{b_{n-1} - b}{b}. \tag{3.25b}$$

For an internal power-law singularity

$$S(\omega) \propto (\omega - \omega_i)^\nu \tag{3.26}$$

at the energy ω_i the reduced perturbation shows a damped oscillation [32]

$$\alpha_n \overset{n\to\infty}{=} A\frac{\cos(nK_i + \Phi)}{n^{\nu+1}} \tag{3.27a}$$

$$\cos K_i = \frac{\omega_i - a}{2b}. \tag{3.27b}$$

The position of the singularity is connected to the frequency of the oscillation. The degree of the singularity is connected to the damping . In principal the four coefficients can be obtained by a least-squares fit to the computed reduced perturbation. Equations. (3.27a), (3.27b) are results from a first order perturbation consideration in the reduced perturbation. In this linearized regime, the effect of different singularities will be a sum of damped oscillations of the type discussed above [33].

Chapter 4

Nearest Neighbour Toy Model

To gain some qualitative understanding of the spectral density, I studied a simplified toy model. The triplon is a spin 1 particle with three different flavours (t^1,t^0,t^{-1}). In this toy model the particles have no flavour, no spin and can hop only to the adjacent site on the chain [34]. This defines the one-particle Hamiltonian H_1. In the two-particle sector an additional interaction is laid onto particles on adjacent sites (H_2). If there are three particles the main contribution is expected to stem from the process which lowers the energy of three particles on three neighbouring sites (H_3). The action of the full transformed spin ladder Hamiltonian is local in real space for $x < 1$. The terms incorporated into the toy model are also the most important terms in the original spin ladder Hamiltonian. So only the hopping to nearest sites and local many particle contributions is incorporated. The hardcore constraint is built into the Hamiltonian by switching to spinless fermionic operators $c_r^\dagger, c_r$. This ensures that no site is excited twice. The hardcore constraint is incorporated already in the commutator.

The Hamiltonian reads

$$
\begin{aligned}
H &= H_1 + H_2 + H_3 && (4.1a)\\
H_1 &= \sum_r t(c^\dagger_{r+1} c_r + c^\dagger_{r-1} c_r) && (4.1b)\\
H_2 &= \sum_r u c^\dagger_{r+1} c^\dagger_r c_{r+1} c_r && (4.1c)\\
H_3 &= \sum_r v c^\dagger_{r+2} c^\dagger_{r+1} c^\dagger_r c_{r+2} c_{r+1} c_r . && (4.1d)
\end{aligned}
$$

The hopping amplitude t is positive and the two- and three particle interactions (u, v) are non-positive.
In optical absorption experiments the excited triplons are local in space. Therefore the initial state is chosen to be as local as possible in real space.

For this reason the relative distances are set to $d_i = 1$. Then for one, two and three particles the initial states read

$$\begin{aligned}
\mathcal{O}|0\rangle &= |K\rangle \text{ in the one-particle sector,} && (4.2a)\\
\mathcal{O}|0\rangle &= |K, d=1\rangle \text{ in the two-particle sector and} && (4.2b)\\
\mathcal{O}|0\rangle &= |K, d_1=1, d_2=1\rangle \text{ in the three-particle sector.} && (4.2c)
\end{aligned}$$

This toy model has a simple structure which allows to derive an analytical description of the spectral density and the bound state for less than three particles. For three particles the spectral density is evaluated using a tridiagonalisation scheme on a computer. The behaviour at the band edges of the spectral density can be extracted from this toy model which also holds also for the spectral density of the spin ladder Hamiltonian.

4.1 One-particle sector

The results presented in the second chapter Eqs. (2.20) and (2.23e) are used, by setting the hopping amplitude t_d to $t_d = t\delta_{1,d}$. The action of the Hamiltonian on the Fourier-transformed $|K\rangle$ of the position state $|r\rangle$ is

$$H|K\rangle = \underbrace{2t\cos(K)}_{\omega(K)}|K\rangle. \tag{4.3}$$

The dispersion is diagonal in momentum space and of cosine shape. The spectral density is therefore a delta function

$$S(K,\omega) = \delta(\omega - \omega(K)). \tag{4.4}$$

4.2 Two-particle sector

The full spin ladder hopping amplitude describing H_2 is reduced to $t_{d;r'd'} = u\delta_{d,1}\delta_{r',0}\delta_{d',1}$, i.e. the energy for two neighbouring particles is lowered by u. Using the previous results, e.g. Eqs. (2.28), (2.29) and (2.32), one receives for the action of the Hamiltonian on $|K,d\rangle$

$$\begin{aligned}
H|K,d\rangle &= t'|K,d-1\rangle|_{d>1} + u\delta_{d,1}|K,d\rangle + t'|K,d+1\rangle && (4.5a)\\
t' &\equiv 2\cos(\frac{K}{2})t. && (4.5b)
\end{aligned}$$

The total momentum K is conserved while the relative distance d of the two particles is not. This Hamiltonian together with the initial excitation vector $\mathcal{O}|0\rangle = |K,1\rangle$ has the same structure as the Lanczos-recursion formula (3.7)

$$\begin{aligned}
H|q_i\rangle &= b_i|q_{i-1}\rangle + a_i|q_i\rangle + b_{i+1}|q_{i+1}\rangle \text{ for } i \geq 1 && (4.6)\\
|q_1\rangle &= |K,1\rangle. && (4.7)
\end{aligned}$$

Therefore all recursion coefficients can be given directly

$$a_i = u\delta_{i,1}, \tag{4.8a}$$
$$b_i = t'. \tag{4.8b}$$

All coefficients a_i, b_i are constant for $i > 1$. So the Green's function

$$G(K,\omega) = \langle K,1|\frac{1}{\omega - H}|K,1\rangle \tag{4.9}$$

can be evaluated using the square root terminator τ (3.20) in the continued fraction

$$G(K,\omega) = \frac{\langle K,1|K,1\rangle}{\omega - u - t'^2\tau} \tag{4.10a}$$
$$= \begin{cases} \frac{2}{\omega-2u-\sqrt{\omega^2-4t'^2}} & \text{for } \omega \leq -2|t'| \\ \frac{2}{\omega-2u+\sqrt{\omega^2-4t'^2}} & \text{for } \omega \geq 2|t'| \\ \frac{2}{\omega-2u+i\sqrt{4t'^2-\omega^2}} & \text{for } \omega^2 \leq 4t'^2. \end{cases} \tag{4.10b}$$

The Green's function contains all information about the spectral density and possible bound states.
The spectral density is given by the imaginary part of the Green's function

$$S(K,\omega) = -\frac{1}{\pi}\Im G(K,\omega) \tag{4.11}$$
$$= \begin{cases} \frac{\sqrt{4t'^2-\omega^2}}{2\pi(t'^2-u\omega+u^2)} & \text{for } \omega^2 \leq 4t'^2 \\ 0 & \text{otherwise} \end{cases} \tag{4.12}$$
$$= \begin{cases} \frac{\sqrt{16\cos^2(K/2)t^2-\omega^2}}{2\pi(4\cos^2(K/2)t^2-u\omega+u^2)} & \text{for } \omega^2 \leq 16t^2\cos^2(K/2) \\ 0 & \text{otherwise .} \end{cases} \tag{4.13}$$

The band edges of the continuum are $\pm 4t\cos(K/2)$. The two-particle interaction H_2 does not change the position of the band edges in the two-particle sector (see Fig. 4.1). The behaviour at the band edges $S(K,\omega) \propto \sqrt{\omega}$, $\forall u \in \mathbb{R}$ is quite remarkable. For $u = 0$ the particles only interact via the hardcore constraint, i.e. the limitation of the hopping to unoccupied sites. The hardcore constraint changes the spectral density completely. If there is no hardcore constraint the total energy of two particles with total momentum K and relative momentum q is just the sum of the dispersions

$$\omega(K,q) = 2t\left(\cos(K/2-q) + \cos(K/2+q)\right). \tag{4.14}$$

For this hardcore-free system the spectral density at $K = 0$ is

$$\begin{aligned} S_{\text{free}}(K=0,\omega) &= \int_{-\pi}^{\pi} \frac{dq}{2\pi}\delta(\omega - 4t\cos(q)) && \text{(4.15a)} \\ &= \sum_{q\in\{\pm\arccos(\omega/4t)\}} \frac{1}{2\pi|4t\sin(q)|} && \text{(4.15b)} \\ &= \frac{1}{4\pi t\sqrt{1-(\omega/4t)^2}} && \text{(4.15c)} \end{aligned}$$

Comparing this to the spectral density of the system *with* hardcore interaction

$$S(K=0,\omega)|_{u=0} = \frac{\sqrt{1-(\omega/4t)^2}}{2\pi t} \tag{4.16}$$

shows that the hardcore constraint does not change the position of the band edges ($\omega = \pm 4t$), but the behaviour from $1/\sqrt{\omega}$ to $\sqrt{\omega}$ (see Fig. 4.1). This also holds for arbitrary momentum K. The position of the band edges is determined by the free particle behaviour. The hardcore constraint can be viewed as a local perturbing operator. This operator does not change the eigenstates of the Hamiltonian, but the eigenstates obtain a phase. This phase shifts weight in the spectral density. So the behaviour of spectral density at the band edges is changed by the hardcore constraint.
An additional two-particle interaction in the two-particle sector does not change the square root singularity at the band edges. The action of H_2 shifts weight to the lower band edge (see Figs. 4.1 and 4.3) and into the bound state. The positions of the band edges are not altered by the action of H_2. For $u = 0$ the spectral density (see Eq. (4.13)) is singular at the point $K = \pi$. The two particle interaction lowers this singularity of the spectral density to some finite value.

4.2.1 Bound state

Poles of the Green's function on the real axis correspond to eigenstates with energy $\omega_B \in \mathbb{R}$

$$G(K,\omega) = \frac{1}{\omega - \omega_B}. \tag{4.17}$$

The eigenstates is calculated by using the Green's function (4.10b)

$$\begin{aligned} \omega_B &= u + \frac{t'^2}{u} \\ &= u + \frac{4t^2\cos^2(\frac{K}{2})}{u} \quad \text{with } \forall K \in [2\arccos(-u/2t), \pi]. && \text{(4.18)} \end{aligned}$$

For an attractive interaction H_2 ($u < 0$) a bound state forms below the continuum at the boundaries of the Brillouin zone ($\pm\pi$) (see Fig. 4.2). The

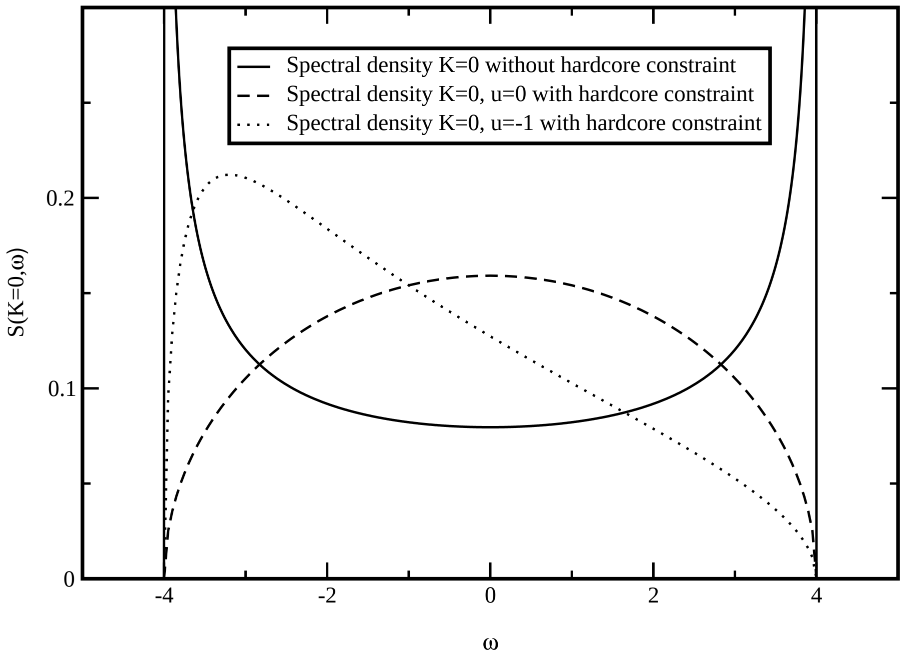

Figure 4.1: Two particle spectral density at $K = 0$ for particles with and without the hardcore constraint. The hardcore constraint determines the behaviour of $S(\omega)$ at the band edges ($S(\omega) \propto \sqrt{\omega}$). Without the hardcore constraint, the behaviour of $S(\omega)$ at the band edges is $S(\omega) \propto (\sqrt{\omega})^{-1}$. The position of the band edges can be determined by the sums of free particle dispersions neglecting the hardcore constraint.

stronger the attractive interaction u is, the lower the bound state lies in energy. If $u < -2t$ holds the bound state lies strictly below the continuum for all momenta. Otherwise the bound state merges into the continuum at the lower band edge at the position $\omega = -2u$ and $q_{\text{merge}} = 2\arccos(-u/2t)$. At the point $(q_{\text{merge}}, \omega = -2u)$ where the bound state merges into the continuum the quality of a bound state is lost. It can decay into continuum-states consisting of two particles with the same energy and the same total momentum. The spectral density has its maximum just slightly above the energy where the bound state merges into the continuum (see Fig. 4.3).
The spectral weight I_B of the bound state can be calculated by

$$\frac{1}{I_B} = \partial_\omega \frac{1}{G}|_{\omega=\omega_B} \tag{4.19}$$

$$\Rightarrow I_B = 1 - \left(\frac{t'}{u}\right)^2$$

$$= 1 - 4\left(\frac{t\cos(K/2)}{u}\right)^2. \tag{4.20}$$

The spectral weight of the bound state has its maximum at the boundary of the Brillouin zone $K/\pi = \pm 1$. The spectral weight vanishes when the bound state merges into the continuum. For increasing u more spectral weight is shifted into the bound state (see Fig. 4.3) and the maximum of the spectral density decreases.

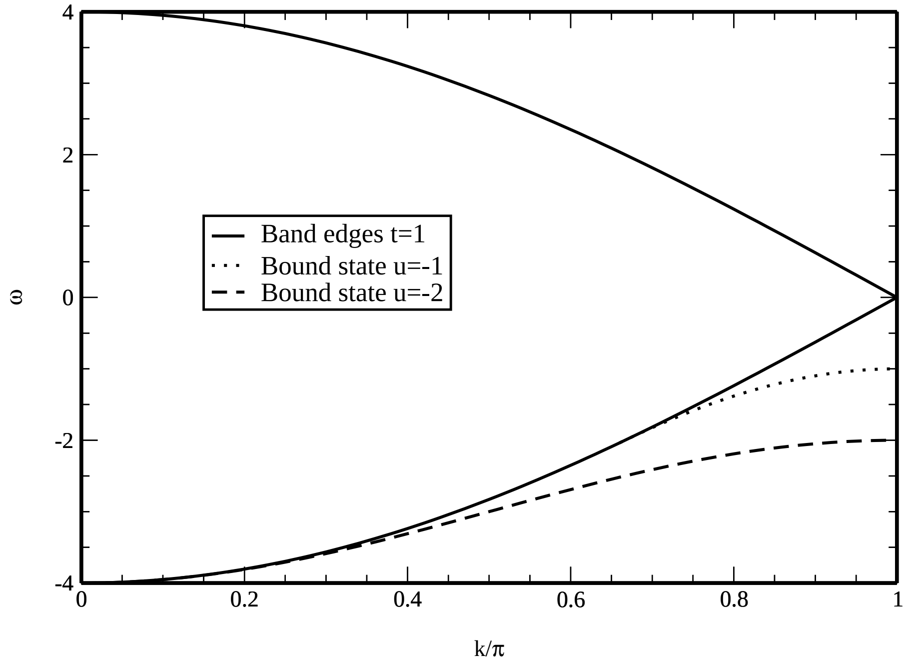

Figure 4.2: Band edges of the two-particle continuum for $t = 1$. The positions of the bound states for $u = -1$ and $u = -2$ are shown. The $u = -2$ bound state merges into the continuum at $k = 0$. The $u = -1$ bound state merges into the continuum at $k/\pi = 2\arccos(u/2t) \approx 0.66$.

4.3 Three-particle sector

If three particles are present in the system the Hamiltonian does not show the simple structure as in the one- or two particle-sectors. But the position of the band edges can be calculated without solving the full toy model.

4.3.1 Position of the band edges

The position of the band edges of the three particle continuum can be calculated from the dispersion (4.3) and the bound state (4.18) by finding the extrema of

$$(\omega(q1) + \omega(q2) + \omega(q3))|_{q1+q2+q3 \equiv K} \tag{4.21}$$

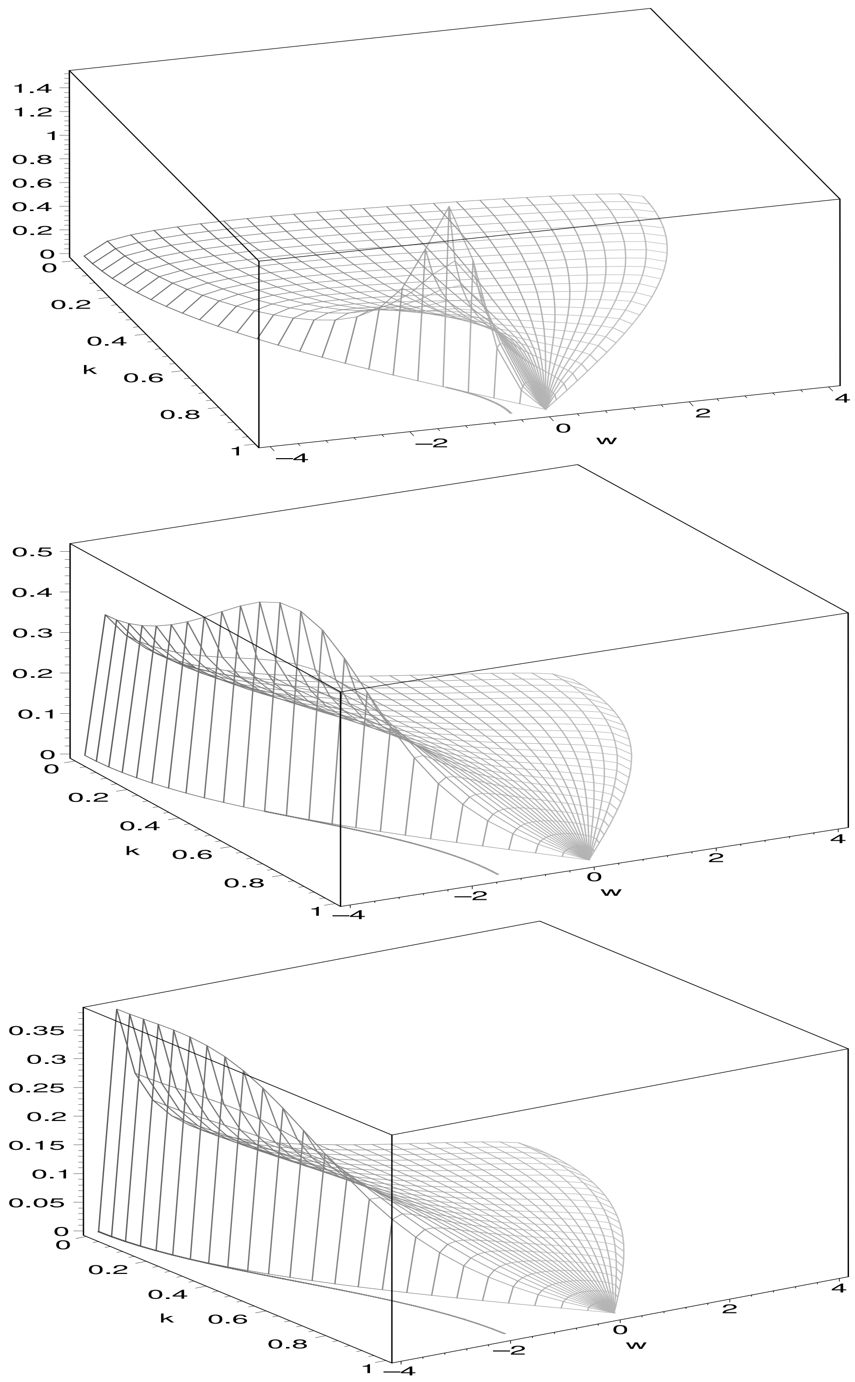

Figure 4.3: Two-particle continuum for $t = 1$ and $u = -0.5$ (top), $u = -1.5$ (middle) and $u = -2$ (bottom). The momentum is measured in units of π. The energy axis is labeled with w. The position of the bound states is sketched as solid black lines below the continuum. The $u = -2$ bound state merges into the continuum at $k = 0$. The spectral weight is shifted towards the lower band edge by the attractive $u < 0$. The spectral density has its maximum just slightly above the lower band edge, where the bound state merges.

and

$$(\omega_B(q1) + \omega(q2))|_{q1+q2\equiv K} \text{ with } q_1 \in [q_{\text{merge}}, \pi] \tag{4.22}$$

with respect to the relative momenta q_i. The extrema of the three dispersions (see Fig. 4.4) are

$$\omega(K) \in \left\{6t\cos(\frac{K + 2\pi n'}{3}) \text{ with } n' \in \{0, 1, 2\}; -2t\cos(K)\right\}. \tag{4.23}$$

The band edges of $H_1|_3$ are $6t\cos(\frac{K+2\pi}{3})$ and $6t\cos(\frac{K}{3})$. The other two extrema lie in the continuum.

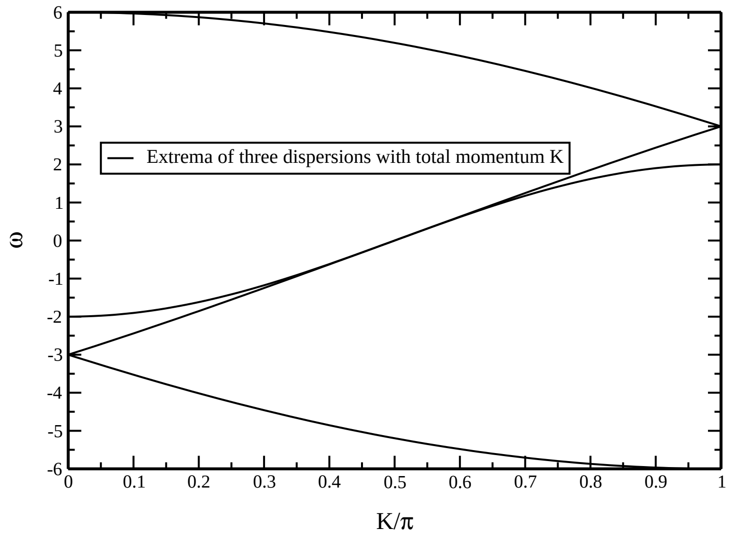

Figure 4.4: Extrema of three free dispersions ($t = 1$) with total momentum K. The lowest and uppest curve are the band edges for $u = 0$.

In the three particle sector one bound state of two particles and a third particle form a continuum. For $u < -t$ this continuum lies partly below the continuum formed by three free particles. In order to find the band edges of the three particle continuum of $H_1|_3 + H_2|_3$ the band edges of the three free ($u = 0$, no hardcore constraint) particle continuum and the one particle plus bound state continuum have to be compared (see Figs. 4.5, 4.6 and 4.7). The extrema of one-particle dispersion and the two-particle bound state are computed numerically. The bound state ω_B exists only for values of $q_1 \in [q_{\text{merge}}, \pi]$. If the attractive two particle interaction u is smaller than $-2t$ a bound state exists for all momenta in the two particle sector.
At the point $(q_{\text{merge}}, \omega = -2u)$ where the bound state merges into the two particle continuum the quality of a bound state is lost. Therefore the part of the edges of the three particle continuum where one particle and a bound state can occur have to be split into two parts (see Figs. 4.5, 4.6 and 4.7

). In one part the bound state lies in the two-particle sector strictly below the two particle continuum and in Eq. (4.22) the relative momentum is $q_1 \in]q_{\text{merge}}, \pi]$ (dashed line) . The other part of the three particle band edge consists of the bound state at the position $q_1 = q_{\text{merge}}$ where it decays into the two particle continuum states (dotted lines in the Figs. 4.5 and 4.6).
All figures are plotted for $t = 1$. For $u = -0.5$, the bound state plus free particle band edges lie completely in the three free particle continuum (see Fig. 4.5).
For $u = -1.5$, the lower band edge of the bound state plus free particle continuum lies for $0 \leq K < 0.3\pi$ below the three free particle continuum.
For $u = -2$, the bound state plus free particle lower edge lies for $0 \leq K < \pi$ below the three free particle continuum. At the lower band edge at $K = \pi$, the bound state merges into the two-particle continuum, otherwise the two-particle bound state lies strictly below the two- particle continuum.

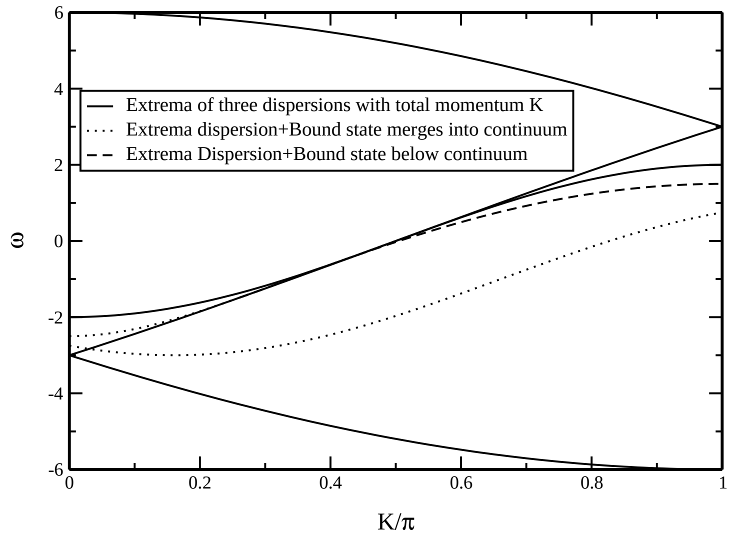

Figure 4.5: The band edges of the the bound state plus free particle continuum are plotted for (inter-)action strengths ($t = 1$, $u = -0.5$). The extrema of the sum of three dispersions with total momentum K are plotted as solid lines.

4.3.2 Form of the spectral density

The three particles are denoted by the absolute position of the particle with the smallest position on the chain r and the relative distances d_1, d_2. So the position state reads $|r, r + d_1, r + d_1 + d_2\rangle$. The momentum state is the Fourier-transformed of the position state with a phase in the exponential

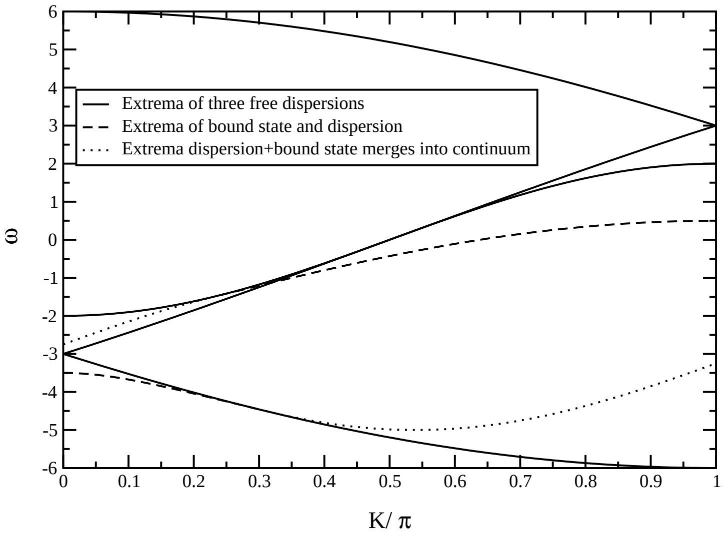

Figure 4.6: The band edges of the the bound state plus free particle continuum are plotted for (inter-)action strengths ($t = 1$, $u = -1.5$). The extrema of the sum of three dispersions with total momentum K are plotted as solid lines.

according to the center of mass

$$|K, d_1, d_2\rangle = \sum_r \exp\Big(iK(r + \frac{2d_1 + d_2}{3})\Big)|r, r + d_1, r + d_1 + d_2\rangle \qquad (4.24)$$

The action of H on the momentum state (4.24) is

$$\begin{aligned} H &= H_1 + H_2 + H_3 && (4.25)\\ H_1|K, d_1, d_2\rangle &= h|K, d_1 + 1, d_2\rangle + \overline{h}|K, d_1, d_2 + 1\rangle \\ &+ \Big(\overline{h}|K, d_1 - 1, d_2\rangle + h|K, d_1 - 1, d_2 + 1\rangle\Big)|_{d1>0} \\ &+ \Big(\overline{h}|K, d_1 + 1, d_2 - 1\rangle + h|K, d_1, d_2 - 1\rangle\Big)|_{d2>0} && (4.26) \end{aligned}$$

The phase h is $h = te^{iK/3}$ and $\overline{h}$ is the complex conjugated of h. The two- and three-particle contribution H_2 to the Hamiltonian are

$$\begin{aligned} H_2|K, d_1, d_2\rangle &= u\Big(|K, 1, d_2\rangle + |K, d_1, 1\rangle\Big), && (4.27)\\ H_3|K, d_1, d_2\rangle &= v|K, 1, 1\rangle. && (4.28) \end{aligned}$$

The two relative distances $d_1, d_2 > 0$ span a two dimensional parameter space. So each vector $|K, d_1, d_2\rangle$ with fixed total momentum K can be depicted as a two dimensional lattice $\mathbb{N}^2$ with complex occupation numbers

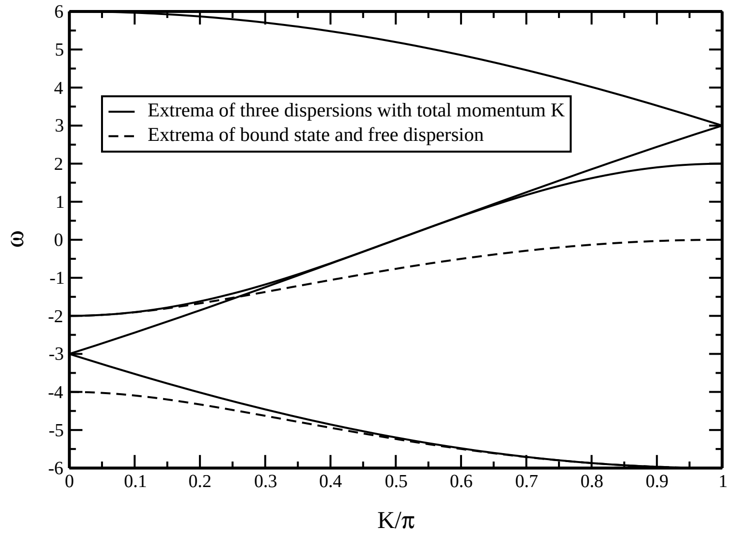

Figure 4.7: The band edges of the the bound state plus free particle continuum are plotted for (inter-)action strengths ($t = 1$, $u = -2$). For $u = -2$ the bound states in the two particle continuum lies strictly below the two-particle continuum for all momentum except $q_1 = 0$.

(see Fig. 4.8). The action of H_1 describes a nearest neighbour hopping of *one* particle in the direction of the axis and diagonal between the axis in the first quadrant ($d_1, d_2 > 0$). The motion of a free (no hardcore constraint) particle would lead to a jump at the band edges of the spectral density. The calculation of the spectral density of $H_1|_3$ shows that the band edges exhibit a cubic behaviour in ω (see Fig. 4.9). I will show that the cubic behaviour has its origin in the hardcore constraint.

The behaviour at the band edges for free hardcore bosons ($u, v = 0$) interacting only through the hardcore-constraint can be understood in the language of fermions. In the fermionic language the hardcore constraint is equivalent to the Pauli-principle which is incorporated in the anticommutation relations for the creation and annihilation operators

$$\{c^\dagger_\alpha, c_\beta\} = \delta_{\alpha,\beta}, \tag{4.29a}$$

$$\{c^\dagger_\alpha, c^\dagger_\beta\} = 0, \tag{4.29b}$$

$$\{c_\alpha, c_\beta\} = 0. \tag{4.29c}$$

First I will show how the square root behaviour is obtained for the two particle continuum. If the two particle state $|K, d = 1\rangle$ is rewritten in the new basis $\{|K, q\rangle = c^\dagger_{K-q} c^\dagger_q |0\rangle\}$ of relative momentum q and the anticommutation

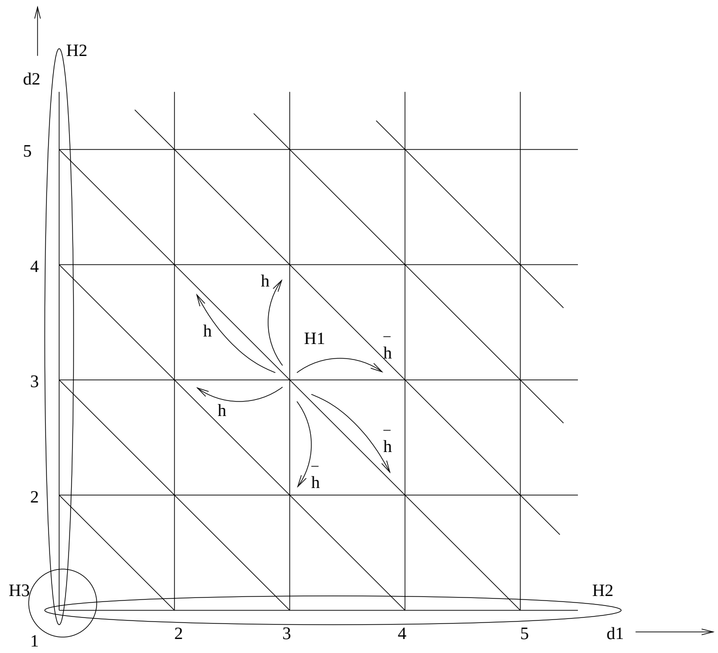

Figure 4.8: The relative distances d_1, d_2 span a two dimensional parameter space for the vectors $|K, d_1, d_2\rangle$ (fixed total momentum). The action of the H_1 describes a nearest neighbour hopping in the direction of the axis and along the depicted diagonal. The operator H_2 lowers the $d_1 = 1$ or $d_2 = 1$ configurations. The three particle interaction acts only on the site $d_1 = d_2 = 1$.

relation (4.29b) is exploited, one finds

$$
\begin{aligned}
|K, d=1\rangle &= \frac{1}{\sqrt{N}} \sum_r \exp\Big(iK(r+1/2)\Big) c^\dagger_{r+1} c^\dagger_r |0\rangle && (4.30a)\\
&= \sum_q \Gamma(q) c^\dagger_{K/2+q} c^\dagger_{K/2-q} |0\rangle \text{ with} && (4.30b)\\
\Gamma(q) &= -i \sin(q). && (4.30c)
\end{aligned}
$$

The factor $\Gamma(q)$ expresses that the particles cannot be in the same state ($c^\dagger_{K/2} c^\dagger_{K/2} = -c^\dagger_{K/2} c^\dagger_{K/2} = 0$) and that the wave function changes sign under exchange of the particles ($q \to -q$).
In the relative momentum basis the operator H_1 is diagonal

$$
H_1 = \sum_k 2t \cos(k) c^\dagger_k c_k. \tag{4.31}
$$

For this reason the states at the band edges $\pm 4t\cos(K/2)$ of the spectral density correspond to $q = 0$ and $q = \pi$. The factor $\Gamma(q)$ can therefore be

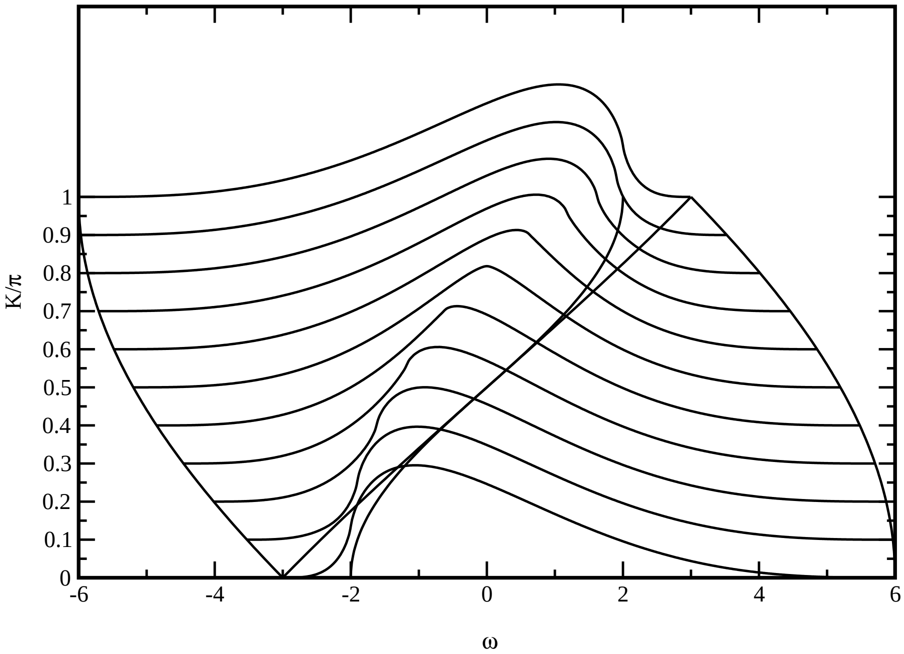

Figure 4.9: Spectral density for $t = 1$ and $u, v = 0$. The band edges behave cubic in ω. The spectral density has a slight kink along the extrema of the total energy calculated from three free particles starting at $K = 0$, $\omega = -2$ and ending at $K = \pi, \omega = 2$.

linearized in the vicinity of the band edges

$$\Gamma(q) \approx \mp iq. \tag{4.32}$$

The spectral density can be obtained by taking the derivative of the total number of excitations

$$\begin{aligned} N(K,\omega) &= \langle K, d=1|\Theta(\omega - H)|K, d=1\rangle \qquad (4.33) \\ &= \sum_q |\langle K, q|K, d=1\rangle|^2 \Theta(\omega - E(K,q)) \\ &= \sum_q |\Gamma(q)|^2 \Theta(\omega - E(K,q)) \end{aligned}$$

with respect to ω. The derivative of the step function $\Theta(\omega - H)$ is a delta function $\delta(\omega - H)$. At the band edges the total energy

$$E(K,q) \in \{\pm 2t(\cos(K/2 - q) + \cos(K/2 + q)) \tag{4.34}$$

is quadratic in q. Within these approximations the band edge behaviour of the spectral density for two free hardcore bosons can be calculated

$$
\begin{aligned}
S_{2T}(K,\omega) &= \frac{dN(K,\omega)}{d\omega} && (4.35a)\\
&\propto \frac{d}{d\omega}\int_q dq \underbrace{q^2}_{|\Gamma(q)|^2}\\
&\propto \frac{d}{d\omega}q^3 \propto \frac{d}{d\omega}\omega^{3/2} \propto \omega^{1/2}.
\end{aligned}
$$

This result was already obtained by a direct calculation of the spectral density in the previous section (Eq. (4.13)).
For three particles I cannot give an analytical expression but the same fermionic approach can be used to explain why the band edges are suppressed by the hardcore constraint. The difference is now that there are two relative distances and thus two relative momenta. The initial vector in the relative momentum basis reads

$$
\begin{aligned}
|K,1,1\rangle &= \sum_{q_1,q_2}\Gamma(q_1,q_2)c^{\dagger}_{K/3+q_1}c^{\dagger}_{K/3+q_2}c^{\dagger}_{K/3-q_1-q_2}|0\rangle && (4.36a)\\
\Gamma(q_1,q_2) &\propto \sin(q_1-q_2)\sin(q_1+2q_2)\sin(2q_1+q_2). && (4.36b)
\end{aligned}
$$

For q_1 ,$q_2 \to 0$ the upper band edge $6t\cos(K/3)$ is approached and the three sine-functions in the factor $\Gamma(q_1,q_2)$ can be linearized for small q_1,q_2. For $q_1 = \frac{\tilde{q}_1+2\pi}{3}$ and $q_2 = \frac{\tilde{q}_2+2\pi}{3}$ the total energy becomes

$$
\begin{aligned}
E(K,q_1,q_2) &= 2t\Big\{\cos\left(\frac{K+2\pi+\tilde{q}_1}{3}\right)+\cos\left(\frac{K+2\pi+\tilde{q}_2}{3}\right)\\
&\quad +\cos\left(\frac{K-4\pi-\tilde{q}_1-\tilde{q}_2}{3}\right)\Big\} && (4.37)
\end{aligned}
$$

which corresponds to the lower band edge $6t\cos(\frac{K+2\pi}{3})$ for $\tilde{q}_1,\tilde{q}_2 = 0$. In the factor

$$
\Gamma(\tilde{q}_1,\tilde{q}_2) \propto \sin\left(\frac{\tilde{q}_1-\tilde{q}_2}{3}\right)\sin\left(\frac{\tilde{q}_1+2\tilde{q}_2}{3}\right)\sin\left(\frac{2\tilde{q}_1+\tilde{q}_2}{3}\right) \qquad (4.38)
$$

the three sines can also be linearized for small $\tilde{q}_1,\tilde{q}_2$. So at the upper and the lower band edge the factor $\Gamma(q_1,q_2)$ or $\Gamma(\tilde{q}_1,\tilde{q}_2)$ is cubic in the relative momenta and the total energy is quadratic. The band edge behaviour of the spectral density for three free hardcore bosons can then be calculated

$$
\begin{aligned}
S_{3T}(K,\omega) &= \frac{dN(K,\omega)}{d\omega} && (4.39)\\
&\propto \frac{d}{d\omega}\iint_{-q}^{q} dq_1 dq_2|\Gamma(q_1,q_2)|^2\\
&\propto \frac{d}{d\omega}\int_0^q dq|q| \quad q^6\\
&\propto \frac{d}{d\omega}q^8 \propto \frac{d}{d\omega}\omega^4 \propto \omega^3.
\end{aligned}
$$

In general, the band edge behaviour for n free hardcore bosons is determined by the power of the factor Γ. Assuming each sine-function can be linearized, then Γ would be proportional to q^η with $\eta = \binom{n}{2} = n(n-1)/2$. The intergration of $|\Gamma|^2$ over the $(n-1)$ relative momenta gives

$$N \propto q^{n^2-1} \propto \omega^{\frac{n^2-1}{2}}. \tag{4.40}$$

Since the energy is quadratic at the band edges, the band edge behaviour of the spectral density is

$$S_n \propto \omega^{\frac{n^2-3}{2}} \text{ for } n > 1. \tag{4.41}$$

At the extremum $-2t\cos(K)$ (4.23) of the three free particle dispersions a slight kink appears in the spectral density (see Fig. 4.9) for vanishing interaction strengths $u, v = 0$. This can be seen at best in the asymptotic behaviour of the recursion coefficients a_i, b_i. A damped oscillation in the reduced perturbation (see Chapter 3) was fitted. The damping of $1/n$ shows that the internal singularity exhibits a linear behaviour in the vicinity of the extrema in momentum space. The other extrema $6t\cos((K+4\pi)/3)$ of the three free particle dispersion (4.23) between the band edges does not lead to a visible singularity in the spectral density (see Fig. 4.9). The position of the maximum of the spectral density for $K = 0$ is $\omega \approx -1.6$ and shifts up in the energy for increasing total momentum until $\omega \approx 1.6$ for $K = \pi$.

If a small interaction $u = -0.5, v = 0$ is turned on, the spectral density changes (see Fig. 4.10). The attractive interaction u on two neighbouring particles shifts spectral weight towards lower energies. The band edge behaviour is cubic as for $u = 0, v = 0$. At the position of the extrema of three free particles $-2t\cos(K)$, where for $u = 0$ a kink appeared , a local maximum is situated nearby. At the upper edge of the continuum of a bound state and a free particle, a jump and a peak structure ($0.6\pi \leq K < \pi$ and $0 \leq K \leq 0.3\pi$) appears in the spectral density. The peak has a Lorentzian form. The limits a, b of the recursion coefficients are approached in a very complex behaviour which made it very difficult to gain information about the analytical behaviour at this point of the spectral density. The damped oscillations around the limits a, b are relatively strong because the damping behaves like $1/n$. This corresponds to the step in the spectral density. Because of this reason, appending the square root terminator gives rise to unphysical wiggles in the spectral density.
At the part of the lower band edge of the bound state and the free particle continuum above the lower band edge formed by three unbound particles

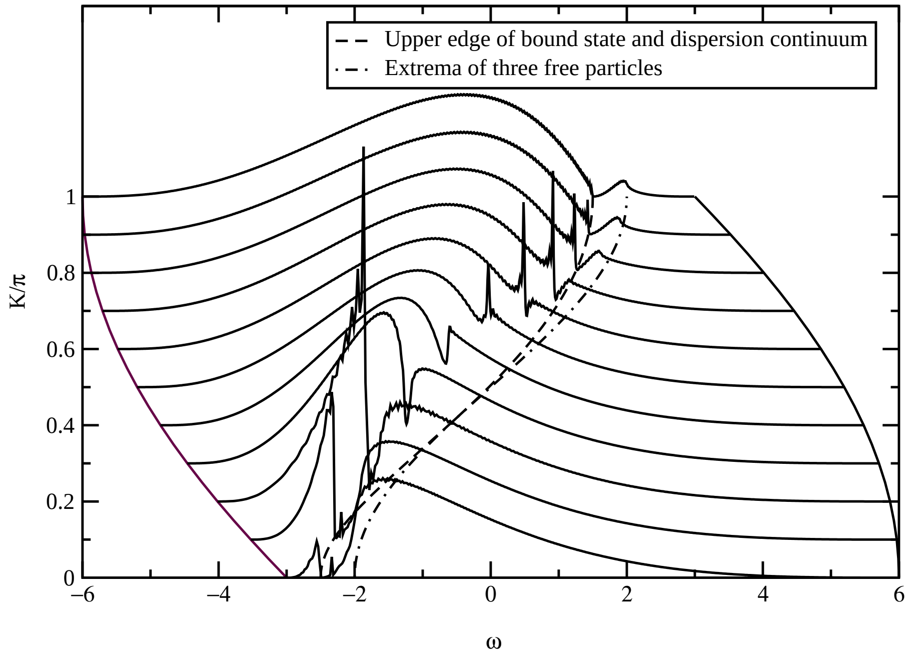

Figure 4.10: Spectral density for interaction strength $t = 1$, $u = -0.5$ and $v = 0$. The total momentum is measured in units of π.

there are no significant structure visible in the spectral density. There the spectral density is smooth and continuous (see Fig. 4.10).
The spectral weight is further lowered towards the lower band edge (see Fig. 4.11) for an interaction strength $u = -1.5$. The lower band edge for $0 \leq K < 0.3\pi$ is given by the lower edge of the bound state plus a free particle continuum (see Fig. 4.6). At this part of the lower band edge the spectral density has a jump. For $K > 0.3\pi$ the behaviour at the lower band edge is cubic, because the lower band edge is given by three hardcore bosons without a bound state. The upper band edge is also cubic. For $K > 0.3\pi$ at the upper edge of the bound state plus free particle continuum a jump with is found. For $K < 0.3\pi$ the extremum $-2t\cos(K)$ approaches the upper band edge of the bound state plus free particle continuum. At this region the step disappears.
For the interaction $u = -2$ almost all spectral weight lies between the edges of the bound state plus free particle continuum (see Fig. 4.12) . At the upper band edge of this latter continuum a jump and a peak occurs for $K < 0.3\pi$. The extremum $-2t\cos(K)$ of three free particles approaches the upper band edge. The lower band edge is given by the lower edge of the bound state plus free particle band edge so no cubic behaviour is expected. Below the continuum lies a three particle bound state which is bound together by the attractive two particle interaction.

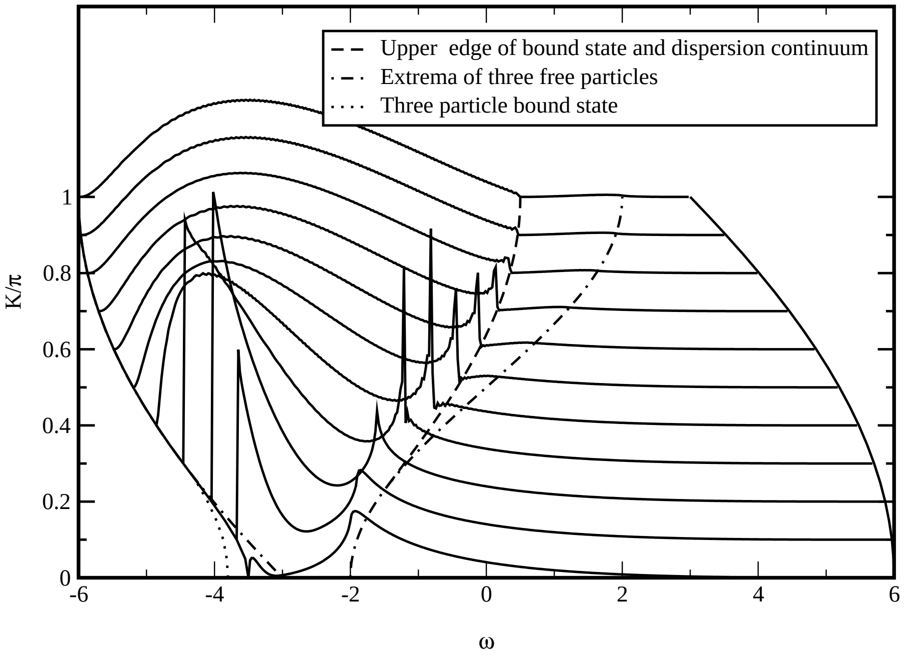

Figure 4.11: Spectral density for interaction strength $t = 1$, $u = -1.5$ and $v = 0$.The total momentum is measured in units of π. For $u = -1.5$ a three particle bound state there is under the continuum.

If the interaction H_2 is set to zero and the three particle interaction strength of H_3 is set to $v = 0.5$ (see Fig. 4.13), then the spectral density is similar to the case where only H_1 is present (see Fig. 4.9). The band edges show a cubic behaviour in ω. The spectral density does not show so much structure as if an attractive two-particle interaction is present. The three-particle interaction shifts weight to lower energies. The kink at the extrema $-2t\cos(K)$ of the three dispersions becomes more pronounced at small total momentum K. The maximum height of the spectral density is bigger for small K as compared to the maximum without any two- and three-particle interactions (see Fig. 4.9).

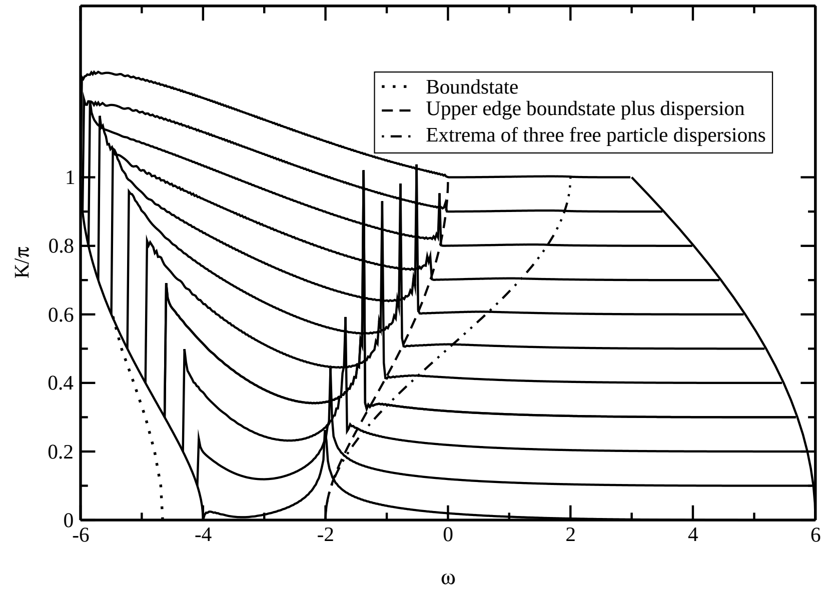

Figure 4.12: Spectral density for interaction strength $t = 1$, $u = -2$ and $v = 0$.The total momentum is measured in units of π. For $u = -2$ a three particle bound state appears under the continuum. The lower band edge is determined by two particle bound state and a single particle. So it does not behave cubic like the upper band edge.

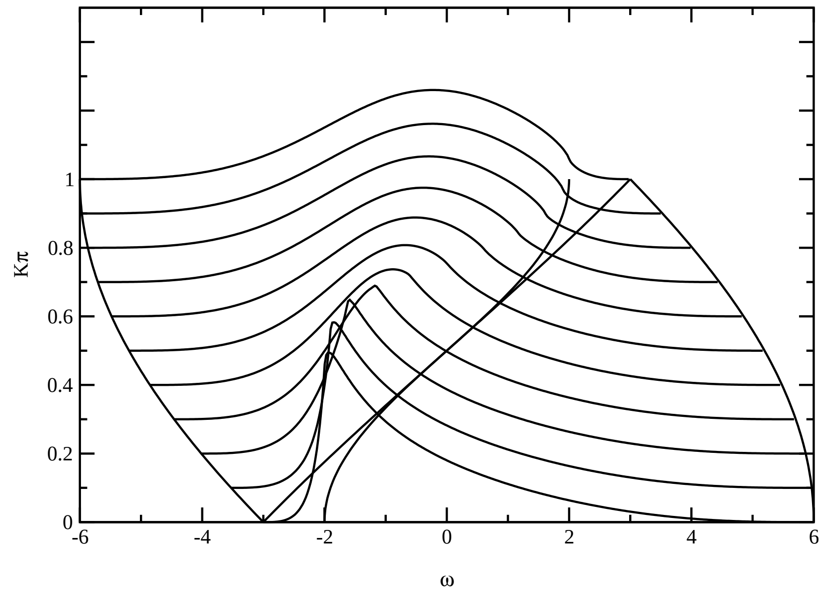

Figure 4.13: Spectral density for interaction strength $t = 1$, $u = 0$ and $v = -0.5$.The total momentum is measured in units of π.

Chapter 5

Three-Triplon Spectral Density

In this chapter the three-triplon spectral density of the spin 1/2 Heisenberg ladder is evaluated. The optical conductivity is calculated for $x = 1.0$. It is shown that the three triplon contribution to $\sigma(\omega)$ has the right energy to give a better description of the optical conductivity of $La_{5.2}Ca_{8.8}Cu_{24}O_{41}$. The spectral density is computed for the case of zero total spin. The spin state of three triplons coupled to total spin $S = 0$ is

$$\begin{aligned}\sqrt{6}|S=0,m=0\rangle &= |t^1,t^0,t^{-1}\rangle - |t^0,t^1,t^{-1}\rangle - |t^{-1},t^0,t^1\rangle \\ &\quad -|t^1,t^{-1},t^0\rangle + |t^0,t^{-1},t^1\rangle + |t^{-1},t^1,t^0\rangle. \quad (5.1)\end{aligned}$$

So each permutation $P_{i,j}$ with $i,j \in \{1,2,3\}$ of two spins gives a factor minus one

$$P_{i,j}|S,m\rangle = -1|S,m\rangle. \quad (5.2)$$

The three triplons are denoted by their positions r, $r+d_1$ and $r+d_1+d_2$. The relative distances between nearest triplons are d_1 and d_2. The triplons are indistinguishable. One possibility to take this into account is to restrict the relative distances d_i to positive values in the position ket $|r,r+d_1,r+d_1+d_2\rangle$. The action of H_1 is specified by the hopping amplitudes t_d, which shifts the three particles separately

$$\begin{aligned}H_1|r,r+d_1,r+d_1+d_2\rangle = \sum_d t_d \Big\{ |r+d,r+d_1,r+d_1+d_2\rangle \\ +|r,r+d_1+d,r+d_1+d_2\rangle + |r,r+d_1,r+d_1+d_2+d\rangle \Big\}. \quad (5.3)\end{aligned}$$

Since d is not restricted there can occur states which violate the notation convention $d_1, d_2 > 0$, e.g. $|r+3,r+1,r+4\rangle|S,m\rangle$. These states have to be restated with exchanged triplons, e.g. $|r+1,r+3,r+4\rangle P_{1,2}|S,m\rangle =$

$-|r+1, r+3, r+4\rangle|S, m\rangle$. States with identical positions are not possible and have to be left out in the summation.
The action of H_2 on the real space state is

$$\begin{aligned} H_2|r, r+d_1, r+d_1+d_2\rangle &= \sum_{r',d'} \Big\{ t_{d_1,r',d'}|r+r', r+r'+d', r+d_1+d_2\rangle \\ &+ t_{d_1+d_2,r',d'}|r+r', r+d_1, r+r'+d'\rangle \\ &+ t_{d_2,r',d'}|r, r+d_1+r', r+d_1+r'+d'\rangle \Big\}, \end{aligned} \tag{5.4}$$

and the action of H_3 reads

$$H_3|r, r+d_1, r+d_1+d_2\rangle = \sum_{r',d'_1,d'_2} t_{d_1,d_2;r',d'_1,d'_2}|r+r', r+r'+d'_1, r+r'+d'_1+d'_2\rangle. \tag{5.5}$$

Furthermore the inversion and translational symmetry of the spin ladder can be used to reduce the number of computations. The symmetries for the hopping amplitudes are

$$t_d = t_{-d} \quad \text{for } H_1, \tag{5.6a}$$
$$t_{d,r',d'} = t_{d,-r'-d'+d,d'} \quad \text{for } H_2 \text{ and} \tag{5.6b}$$
$$t_{d_1,d_2,r',d'_1,d'_2} = t_{d_2,d_1,-r'-d'_1-d'_2+d_1+d_2,d'_2,d'_1} \quad \text{for } H_3. \tag{5.6c}$$

The total momentum state $|K, d_1, d_2\rangle$ is the Fourier-transformed of the position state

$$|K, d_1, d_2\rangle = \sum_r \exp\big(iK(r + \frac{2d_1+d_2}{3})\big)|r, r+d_1, r+d_1+d_2\rangle. \tag{5.7}$$

The action of the Hamiltonian $H = H_1 + H_2 + H_3$ on the state $|K, d_1, d_2\rangle$ is evaluated in the appendix A. The Hamiltonian is implemented as a case differentiation in the tridiagonalization on a computer system.
The observable

$$\mathcal{O}^{\text{leg}}(K)|0\rangle = \sum_{r,l\in\mathbb{Z},d_1,d_2>0} e^{iKr} a_{l,d_1,d_2}|r+l, r+l+d_1, r+l+d_1+d_2\rangle \tag{5.8}$$

is described by the excitation amplitudes a_{l,d_1,d_2}. These amplitudes exhibit the inversion symmetry of the ladder

$$a_{l,d_1,d_2} = -a_{-l-d_1-d_2,d_2,d_1}. \tag{5.9}$$

The minus sign appears because the inversion of the ladder exchanges the particles to the left and to the right. After the reflection about the origin the particle in the middle position is afterwards also in the middle position. The left and the right particle have to be exchanged which gives the factor minus one. The relative distances d_1 and d_2 are also exchanged. Using this symmetry and restating the observable in the momentum basis one finds

$$\begin{aligned}
\mathcal{O}^{\text{leg}}(K)|0\rangle &= \sum_{d_1,d_2>0;2l\geq d_1+d_2} \left(a_{l,d_1,d_2}\left[e^{-iKx}|K,d_1,d_2\rangle - e^{iKx}|K,d_2,d_1\rangle\right]\right), \\
x &= l + \frac{2d_1+d_2}{3}. \qquad (5.10)
\end{aligned}$$

For $K = 0$ all processes which create excitations with $d_1 = d_2$ cancel out. For this reason the spectral density has its smallest contribution at zero total momentum.

The spectral density is calculated for four different values of the exchange coupling $x \in \{0.25, 0.5, 0.75, 1.00\}$. For all these values a bound state appears under the two triplon continuum. Therefore the lower band edge of the three triplon continuum can be given by states consisting of a two triplon bound state and a third unbound triplon. At this part of the lower band edge a jump occurs like in the studied toy model. The other parts of the band edges are cubic in ω. The dispersion has a small dip at $K = 0$ for $x \geq 0.75$. This feature is not incorporated into the toy model. Therefore one can expect a qualitative different behaviour of the spectral density.

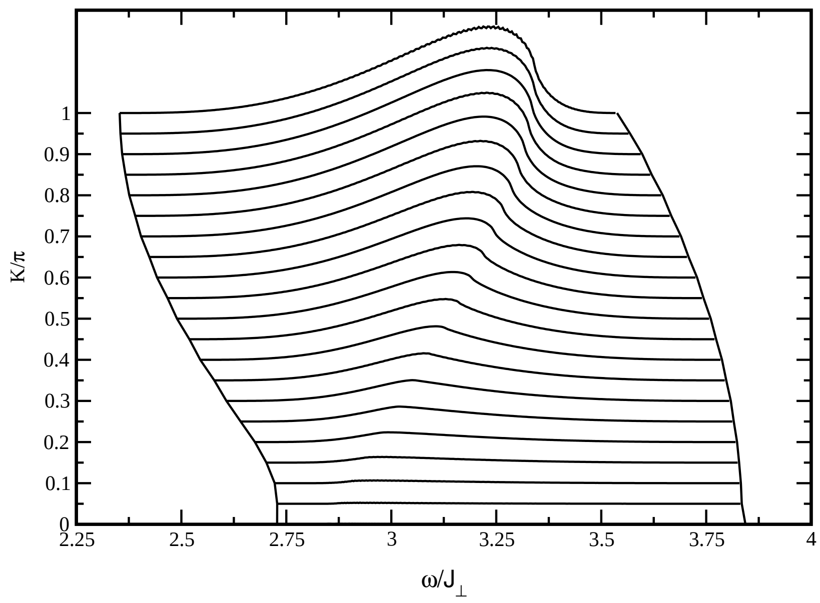

Figure 5.1: Spectral density of $H_1|_3$ for the coupling strength $x = 0.25$. The energy is measured in units of the exchange coupling $J_\perp$, while the total momentum is measured in units of π.

For $x = 0.25$ the spectral density shows a similar behaviour as the toy model (see Figs. 5.1 and 5.3) . In the toy model the observable is not momentum dependent. The major contribution $|K, 1, 1\rangle$ of the observable for small x is proportional to $\sin(K(l + 1))$ (see Eq. (5.10)). So the spectral density has its maximum for $K = \pi$. Taking this into account, one sees that the spectral density has a qualitative very similar behaviour as the toy model spectral density. The Hamiltonian is $H = H_1+H_2+H_3$. I will discuss the contributions of the Hamiltonian separately.
If one considers the one triplon hopping part H_1 one sees (see Fig. 5.1) clearly the same structure as for the toy model density where the two and three particle interactions are set to zero (see Fig. 4.9).
The two triplon interaction H_2 leads to jump in the spectral density (see

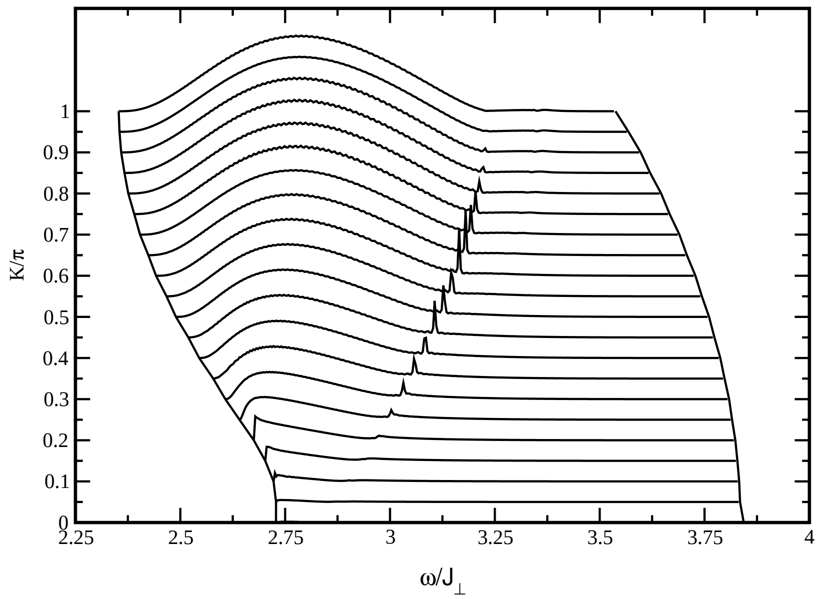

Figure 5.2: The spectral density of $H|_3 = H_1|_3 + H_2|_3$ for the coupling strength $x = 0.25$ depicted.

Fig. 5.2) at the lower band edge due to the possible bound state and a third triplon continuum as described in the last chapter (see Fig. 4.11). The main contribution of the spectral density is centered between the lower band edge and the peak structure at intermediate energies. For intermediate total momentum values the small peak structure is not exactly at the upper edge of the bound state plus unbound triplon continuum for the full Heisenberg ladder. This behaviour of found in the toy model does not hold for the full ladder calculation. The dispersion is no more a simple cosine like in the toy model and further many triplon excitation processes are taken into account in the full calculation. The peak structure is determined by H_1 and H_2. It changes only marginal by a three-particle interaction. The peak is also of Lorentzian form as in the nearest neighbour model. The contributions of

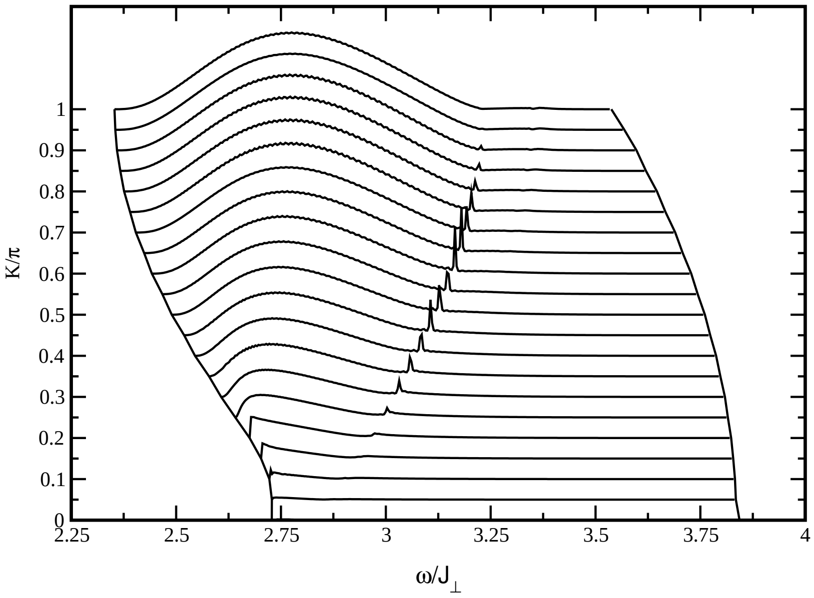

Figure 5.3: Spectral density of $H|_3 = H_1|_3 + H_2|_3 + H_3|_3$ for the coupling strength $x = 0.25$.

H_3 are marginal for $x = 0.25$ (Compare Figs. 5.2 and 5.3). The qualitative behaviour of the spectral density is dominated by H_1 and H_2.

For the coupling strength $x = 0.5$ no new features appear in the spectral density for the Hamiltonian $H = H_1$ compared to $x = 0.25$. The action of H_2 shifts most of the weight between the lower band edge and the upper edge of the bound state plus third triplon continuum (see Fig. 5.4). The peak structure is not as pronounced as in the case for $x = 0.25$. The action of the three triplon part of the Hamiltonian shifts weight towards the lower band edge. So compared to the case for $x = 0.25$ the three particle interaction due to H_3 becomes more significant.

The spectral density for $x = 0.75$ of $H = H_1$ shows a strong van Hove singularity at $K/\pi > 0.7$ (see Fig. 5.5). This is due to the maximum in the dispersion at small K (see Fig. 2.5). The position of the van Hove singularity ($\omega \approx 4.12 \approx 2 \times 1.78 + 0.55 = 4.11$) at $K = \pi$ corresponds to the energy of the gap ($\omega = 0.55$) of the dispersion at $q_1 = \pi$ and two times the value of the energy of the dispersion at $q_1 = -q_2 = 0.3$ ($\omega = 1.78$). The two triplon interaction H_2 dominates the behaviour of the spectral density (see Fig. 5.6). The strong evidence of the van Hove singularity vanishes in the spectral density and the peak structure becomes weaker. At the lower band edge a step occurs at the lower edge of the bound state region, and

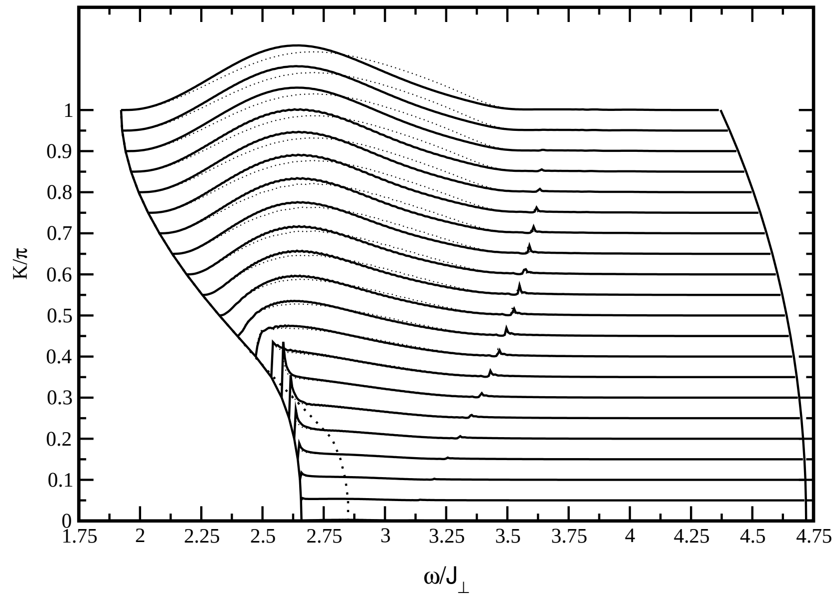

Figure 5.4: Spectral density of $H|_3 = H_1|_3 + H_2|_3 + H_3|_3$ for the coupling strength $x = 0.5$ is shown by solid lines. The spectral density for the Hamiltonian without the irreducible three particle interaction is shown by the light dotted lines. The strong dotted line at the lower band edge depicts the lower band edge of three triplons without any interaction.

a kink ($K/\pi < 0.45$) or a step ($K/\pi = 0.45$) at the lower band edge of three dispersions (dotted line). The effect of H_3 is to shift weight at mainly intermediate and higher momentum values towards the lower band edge.
The spectral density for $x = 1.0$ and $x = 0.75$ without two and three triplon interactions are similar. The van Hove singularity at $K = \pi$ lies at the position of two times the maximum value of the dispersion and the gap value $\omega = 2 * 2.04 + 0.50 \approx 4.6$ (see Fig. 5.7). If the two- and three-particle interactions are incorporated into the Hamiltonian the van Hove singularity disappears (see Fig. 5.8). At $K = 0$, a small structure appears at an energy which is equal to the dispersion at zero momentum plus the two particle bound state energy at momentum π. The wiggles in the curves are due to the complex behaviour of the recursion coefficients.
The optical conductivity (see Eq. 2.36) is calculated using a broadening of $\eta = 0.05J_\perp$ for $x = 1.0$ (see Fig. 5.9). Due to the scaling of the spectral density with a $\sin^4(k/2)$ the most important contributions to the spectral density are those at the boundary of the Brillouin zone. The optical conductivity is compared to the measured $\sigma(\omega)$ [5] of $La_{5.2}Ca_{8.8}Cu_{24}O_{41}$. The three-triplon contribution has the right energy and gives a slightly better description than the mere two-triplon contribution for the optical conductivity.

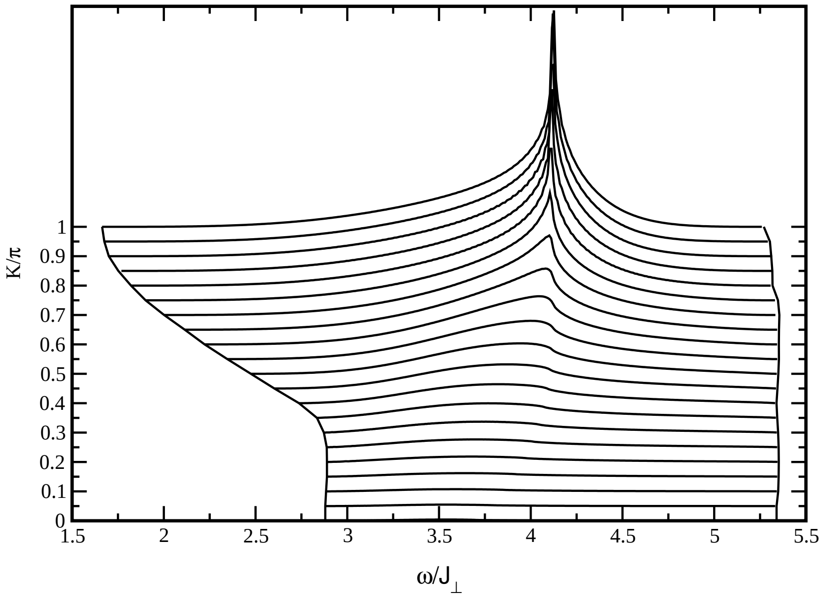

Figure 5.5: Spectral density of $H|_3 = H_1$ for the coupling strength $x = 0.75$ is shown.

The parameter $x = 1.0$ is too small to give the best fit to this experimental data. The best fit is obtained if the ratio of exchange couplings is set to $x \approx 1.2-1.25$ and additional four-spin interactions are also included [24, 35]. Increasing x leads to a spreading of the form of the optical conductivity in the energy. The three triplon contribution becomes more important (see Fig. 2.10) for larger x *and* finite cyclic exchange [5]. It is expected that the three triplon contribution including cyclic exchange corrections and a higher value of the parameter $x = 1.25$ will give a much better description of the experiment.

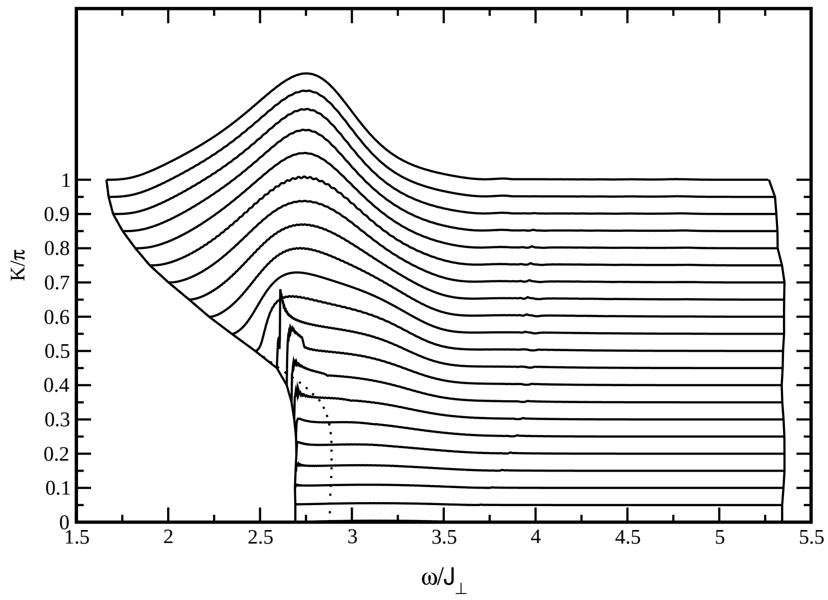

Figure 5.6: The spectral density of $H|_3 = H_1 + H_2 + H_3$ for the coupling strength $x = 0.75$ is shown.The dotted line at the lower band edge depicts the lower band edge of three triplons without any interaction.

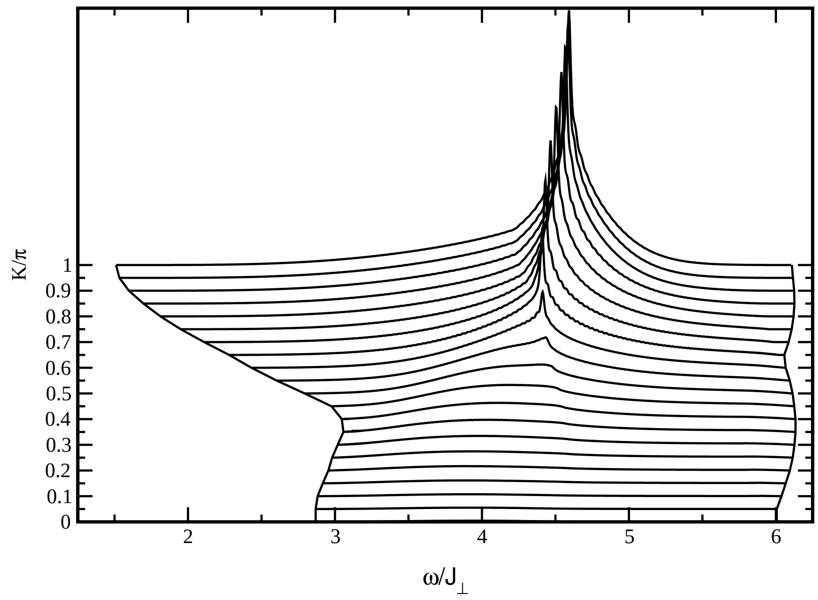

Figure 5.7: The spectral density of $H|_3 = H_1$ for the coupling strength $x = 1.00$ is depicted.

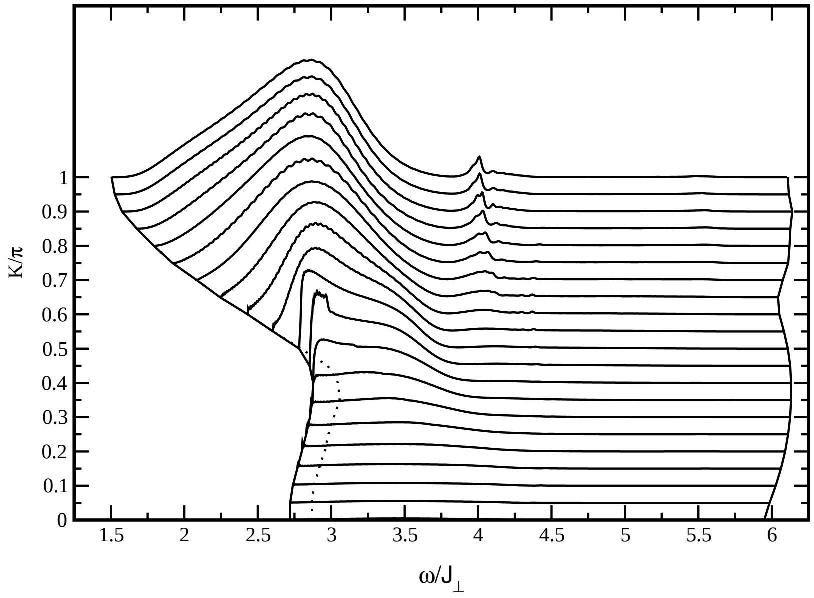

Figure 5.8: The spectral density of $H|_3 = H_1 + H_2 + H_3$ for the coupling strength $x = 1.00$ is shown. The dotted line at the lower band edge depicts the lower band edge of three triplons without any interaction.

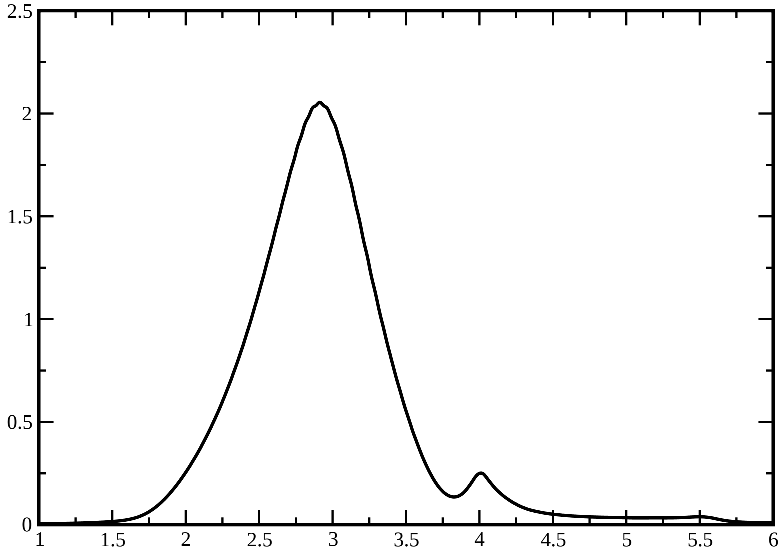

Figure 5.9: The optical conductivity of the three triplon sector for $x = 1.00$ is shown.

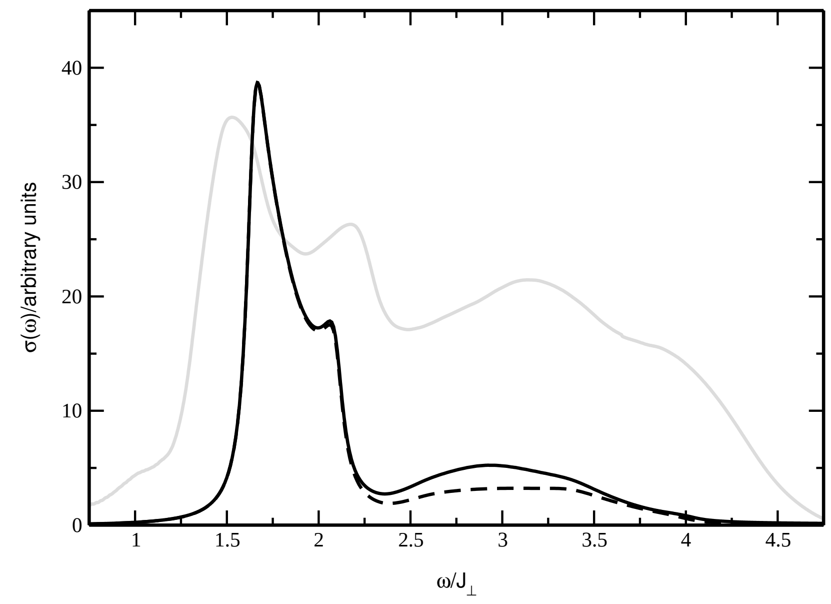

Figure 5.10: Comparison of $\sigma(\omega)$ of $La_{5.2}Ca_{8.8}Cu_{24}O_{41}$ at $T = 4K$ with the calculated contributions by CUT for $x = 1.00$, $J_\perp = 1060\text{cm}^{-1}$, $\omega_{Ph}^{leg} = 570\text{cm}^{-1}$ and a finite broadening $\eta = 0.05J_\perp$. The black dashed line depicts the calculated optical conductivity without the three triplon contribution. The solid black line shows the conductivity including the three triplon contribution (see Fig. 5.9).

Appendix A

The Spin Ladder Hamiltonian

The position r denotes the triplon with the smallest coordinate. The relative distances d_1, d_2 are distance to the next triplon to left. The Fourier transformed of the center of mass is

$$|K, d_1, d_2 >= \frac{1}{\sqrt{N}} \sum_r e^{iK(r+\frac{2d_1+d_2}{3})} |r, r+d_1, r+d_1+d_2 > . \tag{A.1}$$

The one- and and two-triplon (inter-) actions of the Hamiltonian

$$H = H_1 + H_2 + H_3 \tag{A.2}$$

contain processes where the triplons change their order (d_1 or $d_2 < 0$. Since they are indistinguishable they have to be exchanged by the permutation operators P_{12}, P_{23}. The notation convention $d_1, d_2 > 0$ can be fixed as follows

$$|K, -d_1, d_2 > |S.. >= \begin{cases} |K, d_1, d_2 - d_1 > P_{12}|S.. > & d_2 - d_1 > 0 \\ |K, d_2, d_1 - d_2 > P_{23}P_{12}|S.. > & d_1 - d_2 > 0 \end{cases} \tag{A.3}$$

and

$$|K, d_1, -d_2 > |S.. >= \begin{cases} |K, d_2 - d_1, d_1 > P_{12}P_{23}|S.. > & d_2 - d_1 > 0 \\ |K, d_1 - d_2, d_2 > P_{23}|S.. > & d_1 - d_2 > 0. \end{cases} \tag{A.4}$$

This can be seen if the momentum space reprasentation is expressed through real space states

$$|K, -d_1, d_2 > |S.. >= \frac{1}{\sqrt{N}} \sum_r e^{iK(r+\frac{-2d_1+d_2}{3})} |r, r-d_1, r-d_1+d_2 > |S.. > . \tag{A.5}$$

At this point a case differentation has to be done. For $d_2 - d_1 > 0$ one sees

$$\begin{aligned}
&= \frac{1}{\sqrt{N}} \sum_r e^{iK(r+\frac{-2d_1+d_2}{3})} |r-d_1, r, r-d_1+d_2 > P_{12}|S.. > \\
&= \frac{1}{\sqrt{N}} \sum_r e^{iK(r+\frac{d_1+d_2}{3})} |r, r+d_1, r+d_2 > P_{12}|S.. > \\
&= \frac{1}{\sqrt{N}} \sum_r e^{iK(r+\frac{2d_1+(d_2-d_1)}{3})} |r, r+d_1, r+d_1+(d_2-d_1) > P_{12}|S.. > \\
&= |K, d_1, d_2-d_1 > P_{12}|S.. >
\end{aligned}$$

and for $d_1 - d_2 > 0$ holds

$$\begin{aligned}
&= \frac{1}{\sqrt{N}} \sum_r e^{iK(r+\frac{-2d_1+d_2}{3})} |r-d_1, r, r-d_1+d_2 > P_{12}|S.. > \\
&= \frac{1}{\sqrt{N}} \sum_r e^{iK(r+\frac{-2d_1+d_2}{3})} |r-d_1, r-d_1+d_2, r > P_{23}P_{12}|S.. > \\
&= \frac{1}{\sqrt{N}} \sum_r e^{iK(r+\frac{d_1+d_2}{3})} |r, r+d_2, r+d_1 > P_{23}P_{12}|S.. > \\
&= \frac{1}{\sqrt{N}} \sum_r e^{iK(r+\frac{2d_2+(d_1-d_2)}{3})} |r, r+d_2, r+d_2+(d_1-d_2) > P_{23}P_{12}|S.. > \\
&= |K, d_2, d_1-d_2 > P_{23}P_{12}|S.. > .
\end{aligned}$$

The same case differentation has to be done for (A.4). The calculation is

$$|K, d_1, -d_2 > |S.. >= \frac{1}{\sqrt{N}} \sum_r e^{iK(r+\frac{2d_1-d_2}{3})} |r, r+d_1, r+d_1-d_2 > |S.. > \tag{A.6}$$

and for $d_2 - d_1 > 0$ one gets

$$\begin{aligned}
&= \frac{1}{\sqrt{N}} \sum_r e^{iK(r+\frac{2d_1-d_2}{3})} |r, r+d_1-d_2, r+d_1 > P_{23}|S.. > \\
&= \frac{1}{\sqrt{N}} \sum_r e^{iK(r+\frac{2d_1-d_2}{3})} |r+d_1-d_2, r, r+d_1 > P_{12}P_{23}|S.. > \\
&= \frac{1}{\sqrt{N}} \sum_r e^{iK(r-d_1+d_2+\frac{2d_1-d_2}{3})} |r, r-d_1+d_2, r+d_2 > P_{12}P_{23}|S.. > \\
&= \frac{1}{\sqrt{N}} \sum_r e^{iK(r+\frac{-d_1+2d_2}{3})} |r, r-d_1+d_2, r-d_1+d_2+d_1 > P_{12}P_{23}|S.. > \\
&= |K, d_2-d_1, d_1 > P_{12}P_{23}|S.. >
\end{aligned}$$

and for $d_1 - d_2 > 0$

$$
\begin{aligned}
&= \frac{1}{\sqrt{N}} \sum_r e^{iK(r+\frac{2d_1-d_2}{3})} |r, r+d_1-d_2, r+d_1 > P_{23}|S.. > \\
&= \frac{1}{\sqrt{N}} \sum_r e^{iK(r+\frac{2(d_1-d_2)+d_2}{3})} |r, r+(d_1-d_2), r+(d_1-d_2)+d_2 > P_{23}|S.. > \\
&= |K, d_1-d_2, d_2 > P_{23}|S.. > .
\end{aligned}
$$

For total spin 0 each permutation gives a minus sign. So in the following I will not write out the spin part of the states and use the fact that a minus one appears for every permutation needed.

A.1 The Action of $H_1|_3$

is

$$
\begin{aligned}
& H_1|r, r+d_1, r+d_1+d_2 >= 3t_0|r, r+d_1, r+d_1+d_2 > + \\
& \sum_{d\neq 0} t_d \left(\underbrace{|r+d, r+d_1, r+d_1+d_2 >}_{I} + \underbrace{|r, r+d_1+d, r+d_1+d_2 >}_{II} \right. \\
& \qquad \left. + \underbrace{|r, r+d_1, r+d_1+d_2+d >}_{III} \right) .
\end{aligned}
$$

The action of H_1 on the momentum state is given by

$$
H_1|K, d_1, d_2 >= \frac{1}{\sqrt{N}} \sum_r e^{iK(r+\frac{2d_1+d_2}{3})} H_1|r, r+d_1, r+d_1+d_2 > . \quad \text{(A.7)}
$$

The hopping amplitudes have the inversion symmetry of the ladder $t_d = t_{-d}$. This is used for the three different parts I,II and III. Afterwards the notation convention is restored using the above derived equations for negative relative distances. The calculation for the first part I is

$$
\begin{aligned}
&= \sum_{d\neq 0,r} \frac{1}{\sqrt{N}} e^{iK(r+\frac{2d_1+d_2-3d}{3})} t_d |r, r+d_1-d, r+d_1+d_2-d> \\
&= \sum_{d\neq 0,r} \frac{1}{\sqrt{N}} e^{iK(r+\frac{2d_1+d_2+3d}{3})} t_d |r, r+d_1+d, r+d_1+d+d_2> \\
&= \sum_{d\neq 0} e^{iK\frac{d}{3}} t_d \frac{1}{\sqrt{N}} \sum_r e^{iK(r+\frac{2(d_1+d)+d_2)}{3})} |r, r+d_1+d, r+d_1+d+d_2> \\
&= \sum_{d\neq 0} e^{iK\frac{d}{3}} t_d |K, d_1+d, d_2> \\
&= \sum_{d>0} t_d \left(e^{iK\frac{d}{3}} |K, d_1+d, d_2> + e^{-iK\frac{d}{3}} |K, d_1-d, d_2> \right) \\
&= \sum_{d>0} t_d e^{iK\frac{d}{3}} |K, d_1+d, d_2> + \\
&\quad \sum_{d>0} t_d e^{-iK\frac{d}{3}} \begin{cases} |K, d_1-d, d_2> \text{ for } 0<d<d_1 \\ -|K, d-d_1, d_2+d_1-d> \text{ for } d_1<d<d_2+d_1 \\ |K, d_2, d-d_1-d_2> \text{ for } d_1+d_2<d. \end{cases}
\end{aligned}
$$

The same for the second part II gives

$$
\begin{aligned}
& \frac{1}{\sqrt{N}} \sum_{d\neq 0,r} e^{iK(r+\frac{2d_1+d_2}{3})} t_d |r, r+d_1+d, r+d_1+d_2> \\
&= \frac{1}{\sqrt{N}} \sum_{d\neq 0,r} e^{iK(r+\frac{2(d_1+d)+d_2-d}{3})} e^{-iK\frac{d}{3}} t_d |r, r+(d_1+d), r+(d_1+d)+(d_2-d)> \\
&= \sum_{d\neq 0} t_d e^{-iK\frac{d}{3}} |K, d_1+d, d_2-d> \\
&= \sum_{d>0} t_d \left(e^{-iK\frac{d}{3}} |K, d_1+d, d_2-d> + e^{iK\frac{d}{3}} |K, d_1-d, d_2+d> \right) \\
&= \sum_{d>0} t_d e^{-iK\frac{d}{3}} \begin{cases} |K, d_1+d, d_2-d> \text{ for } 0<d<d_2 \\ -|K, d_1+d_2, d-d_2> \text{ for } d_2<d \end{cases} \\
&\quad + \sum_{d>0} t_d e^{iK\frac{d}{3}} \begin{cases} |K, d_1-d, d_2+d> \text{ for } 0<d<d_1 \\ -|K, d-d_1, d_1+d_2> \text{ for } d_1<d. \end{cases}
\end{aligned}
$$

And for the third part III one gets

$$\begin{aligned}
& \frac{1}{\sqrt{N}} \sum_{d\neq 0,r} e^{iK(r+\frac{2d_1+d_2}{3})} t_d |r, r+d_1, r+d_1+d_2+d> \\
= & \frac{1}{\sqrt{N}} \sum_{d\neq 0,r} e^{iK(r+\frac{2d_1+(d_2+d)}{3})} e^{-iK\frac{d}{3}} t_d |r, r+d_1, r+d_1+(d_2+d)> \\
= & \sum_{d\neq 0} e^{-iK\frac{d}{3}} t_d |K, d_1, d_2+d> \\
= & \sum_{0<d} t_d \left(e^{-iK\frac{d}{3}} |K, d_1, d_2+d> + e^{iK\frac{d}{3}} |K, d_1, d_2-d> \right) \\
= & \sum_{0<d} t_d e^{-iK\frac{d}{3}} |K, d_1, d_2+d> \\
& + \sum_{d>0} t_d e^{iK\frac{d}{3}} \begin{cases} |K, d_1, d_2-d> & \text{for } 0<d<d_2 \\ -|K, d_1+d_2-d, d-d_2> & \text{for } d_2<d<d_1+d_2 \\ |K, d-d_1-d_2, d_1> & \text{for } d_1+d_2<d \end{cases}
\end{aligned}$$

A.2 The Action of $H_2|_3$

The symmetry of the hopping amplitudes is

$$t_{d;-r'+\frac{d-d'}{2},d'} = t_{d;r'+\frac{d-d'}{2},d'}. \qquad (A.8)$$

The calculation follows the same route as in the one case for H_1 First calculate the action of H_2 on the momentum states

$$
\begin{aligned}
& H_2|K,d_1,d_2>= \\
= \quad & \frac{1}{\sqrt{N}}\sum_r e^{iK(r+\frac{2d_1+d_2}{3})}\sum_{r',d'}\big(t_{d_1;r',d'}|r+r',r+r'+d',r+d_1+d_2> \\
& +t_{d_1+d_2;r',d'}|r+r',r+d_1,r+r'+d'> \\
& +t_{d_2;r',d'}|r,r+d_1+r',r+d_1+r'+d'>\big) \\
= \quad & \frac{1}{\sqrt{N}}\sum_r e^{iK(r+\frac{2d_1+d_2}{3})}\sum_{r',d'}\Big(t_{d_1;r',d'}e^{-iKr'}|r,r+d',r-r'+d_1+d_2> \\
& +t_{d_1+d_2;r',d'}e^{-iKr'}|r,r-r'+d_1,r+d'> \\
& +t_{d_2;r',d'}|r,r+d_1+r',r+d_1+r'+d'>\big) \\
= \quad & \frac{1}{\sqrt{N}}\sum_{r,r',d'}\Big(e^{iK(r+\frac{2d'+d_1+d_2-r'-d'}{3})}e^{iK\frac{d_1-d'-2r'}{3}} \\
& t_{d_1;r',d'}|r,r+d',r-r'+d_1+d_2> \\
& +e^{iK(r+\frac{2(d_1-r')+d'+r'-d_1}{3})}e^{iK\frac{d_1+d_2-2r'-d'}{3}}t_{d_1+d_2;r',d'}|r,r-r'+d_1,r+d'> \\
& +e^{iK(r+\frac{2(d_1+r')+d'}{3})}e^{iK\frac{d_2-d'-2r'}{3}}t_{d_2;r',d'}|r,r+d_1+r',r+d_1+r'+d'>\Big) \\
= \quad & \sum_{r',d'}\Bigg(\underbrace{e^{iK\frac{d_1-d'-2r'}{3}}t_{d_1;r',d'}|K,d',d_1+d_2-r'-d'>}_{I} \\
& +\underbrace{e^{iK\frac{d_1+d_2-d'-2r'}{3}}t_{d_1+d_2;r',d'}|K,d_1-r',d'-d_1+r'>}_{II} \\
& +\underbrace{e^{iK\frac{d_2-2r'-d'}{3}}t_{d_2;r',d'}|K,d_1+r',d'>}_{III}\Bigg).
\end{aligned}
$$

Afterwards use the symmetry of the hopping amplitudes. The symmetry is used by shifting the sum over r $\hat{r}=-r'+\frac{d1-d'}{2}$. For the first part I one gets

$$
\begin{aligned}
.. \;&=\; \sum_{\hat r; d'>0} t_{d_1;-\hat r+\frac{d_1-d'}{2},d'} e^{iK\frac{2}{3}\hat r}|K,d',d_1+d_2+\hat r-\frac{d_1-d'}{2}-d'> \\
&= \sum_{\hat r\leq 0; d'>0} t_{d_1;-\hat r+\frac{d_1-d'}{2},d'} e^{iK\frac{2}{3}\hat r}|K,d',d_1+d_2+\hat r-\frac{d_1-d'}{2}-d'> \\
&\quad + \sum_{\hat r<0; d'>0} t_{d_1;-\hat r+\frac{d_1-d'}{2},d'} e^{-iK\frac{2}{3}\hat r}|K,d',d_1+d_2-\hat r-\frac{d_1-d'}{2}-d'> \\
&= \sum_{r'\geq\frac{d_1-d'}{2}; d'>0} t_{d_1;r',d'} \underbrace{e^{iK\frac{d_1-d'-2r'}{3}}|K,d',d_1+d_2-r'-d'>}_{I.\alpha} \\
&\quad + \sum_{r'>\frac{d_1-d'}{2}; d'>0} t_{d_1;r',d'} \underbrace{e^{iK\frac{2r'+d'-d_1}{3}}|K,d',d_2+r'>}_{I.\beta}.
\end{aligned}
$$

This $I.\alpha$ can be put into the final form if the notation convention is restored

$$
\begin{aligned}
.. \;&=\; \sum_{r'\geq\frac{d_1-d'}{2},d'} t_{d_1;..} e^{iK\frac{d_1-d'-2r'}{3}}
\begin{cases}
|K,d',d_1+d_2-r'-d'> \\
\text{for } d_1+d_2-r'-d'>0 \\
|K,r'-d_1-d_2,d'> \\
\text{for } d_1+d_2-r'-d'<0 \wedge r'-d_1-d_2>0 \\
-|K,d_1+d_2-r',r'+d'-d_1-d_2> \\
\text{for } d_1+d_2-r'-d'<0 \wedge r'-d_1-d_2<0
\end{cases} \\
&= \sum_{r'\geq\frac{d_1-d'}{2},d'} t_{d_1,r',d'} e^{iK\frac{d_1-d'-2r'}{3}}
\begin{cases}
|K,d',d_1+d_2-r'-d'> \\
\text{for } r'<d_1+d_2-d' \\
|K,r'-d_1-d_2,d'> \\
\text{for } d_1+d_2<r' \\
-|K,d_1+d_2-r',r'+d'-d_1-d_2> \\
\text{for } d_1+d_2-d'<r'<d_1+d_2.
\end{cases}
\end{aligned}
$$

For the second part of the first $I.\beta$ the calculation gives

$$.. \;=\; \sum_{r'>\frac{d_1-d'}{2},d'} t_{d_1;r',d'} e^{iK\frac{2r'-d_1+d'}{3}} \begin{cases} |K,d',d_2+r'> \\ \text{for } d_2+r'>0 \\ |K,-d'-d_2-r',d'> \\ \text{for } d_2+r'<0 \wedge -d'-d_2-r'>0 \\ -|K,d'+d_2+r',-d_2-r'> \\ \text{for } d_2+r'<0 \wedge d'+d_2+r'>0 \end{cases}$$

$$.. \;=\; \sum_{r'>\frac{d_1-d'}{2},d'} t_{d_1;r',d'} e^{iK\frac{2r'-d_1+d'}{3}} \begin{cases} |K,d',d_2+r'> \\ \text{for } -d_2<r' \\ |K,-d'-d_2-r',d'> \\ \text{for } r'<-d_2-d' \\ -|K,d'+d_2+r',-d_2-r'> \\ \text{for } -d_2-d'<r'<-d_2. \end{cases}$$

For the second part one sees that

$$\begin{aligned} .. \;=\; & \sum_{\hat{r};d'>0} t_{d_1+d_2;-\hat{r}+x,d'} e^{iK\frac{2\hat{r}}{3}} |K,d_1+\hat{r}-x,d'-d_1-\hat{r}+x> \\ =\; & \sum_{\hat{r}\leq 0;d'>0} t_{d_1+d_2;-\hat{r}+x,d'} e^{iK\frac{2\hat{r}}{3}} |K,d_1+\hat{r}-x,d'-d_1-\hat{r}+x> \\ & + \sum_{\hat{r}<0;d'>0} t_{d_1+d_2;-\hat{r}+x,d'} e^{-iK\frac{2\hat{r}}{3}} |K,d_1-\hat{r}-x,d'-d_1+\hat{r}+x> \\ =\; & \sum_{r'\geq x;d'>0} t_{d_1+d_2;r',d'} e^{iK\frac{2}{3}(x-r')} \underbrace{|K,d_1-r',d'-d_1+r'>}_{II.\alpha} \\ & + \sum_{r'>x;d'>0} t_{d_1+d_2;r',d'} e^{-iK\frac{2}{3}(x-r')} \underbrace{|K,d_1+r'-2x,d'-d_1-r'+2x>}_{II.\beta}, \end{aligned}$$

which gives for $II.\alpha$

$$.. = \sum_{r' \geq x, d'} t_{d_1+d_2;r',d'} e^{iK\frac{2}{3}(x-r')} \begin{cases} |K, d_1 - r', d' - d_1 + r' > \\ \text{for } d_1 - r' > 0 \wedge d' - d_1 + r' > 0 \\ -|K, r' - d_1, d' - d_1 + r' + d_1 - r' > \\ \text{for } d_1 - r' < 0 \wedge d' - d_1 + r' > 0 \\ -|K, d_1 - r' + d' - d_1 + r', d_1 - d' - r' > \\ \text{for } d_1 - r' > 0 \wedge d' - d_1 + r' > 0 \end{cases}$$

$$= \sum_{r' \geq \frac{d_1+d_2-d'}{2}, d'} t_{d_1+d_2;r',d'} e^{iK\frac{d_1+d_2-d'-2r'}{3}} \begin{cases} |K, d_1 - r', d' - d_1 + r' > \\ \text{for } d_1 - d' < r' < d_1 \\ -|K, r' - d_1, d' > \\ \text{for } d_1 < r' \\ -|K, d', d_1 - d' - r' > \\ \text{for } r' < d_1 - d'. \end{cases}$$

The other part $II.\beta$ is treated in the same way

$$.. = \sum_{r' > \frac{d_1+d_2-d'}{2}, d'} t_{d_1+d_2;r',d'} e^{-iK\frac{d_1+d_2-d'-2r'}{3}} \begin{cases} |K, r' + d' - d_2, d_2 - r' > \\ \text{for } r' + d' - d_2 > 0 \wedge d_2 - r' > 0 \\ -|K, d_2 - r' - d', d' > \\ \text{for } r' + d' - d_2 < 0 \wedge d_2 - r' > 0 \\ -|K, d', r' - d_2 > \\ \text{for } r' + d' - d_2 > 0 \wedge d_2 - r' < 0 \end{cases}$$

$$= \sum_{r' > \frac{d_1+d_2-d'}{2}, d'} t_{d_1+d_2;r',d'} e^{-iK\frac{d_1+d_2-d'-2r'}{3}} \begin{cases} |K, r' + d' - d_2, d_2 - r' > \\ \text{for } d_2 - d' < r' < d_2 \\ -|K, d_2 - r' - d', d' > \\ \text{for } r' < d_2 - d' \\ -|K, d', r' - d_2 > \\ \text{for } d_2 < r'. \end{cases}$$

The third part is calculated like I and two before II and yields

$$
\begin{aligned}
.. &= \sum_{\hat{r};d'>0} t_{d_2;-\hat{r}+x,d'} e^{iK\frac{2\hat{r}}{3}} |K, -\hat{r}+x+d_1, d'> \\
&= \sum_{\hat{r}\leq 0;d'>0} t_{d_2;-\hat{r}+x',d'} e^{iK\frac{2\hat{r}}{3}} |K, -\hat{r}+x+d_1, d'> \\
&\quad + \sum_{\hat{r}<0;d'>0} t_{d_2;-\hat{r}+x',d'} e^{-iK\frac{2\hat{r}}{3}} |K, \hat{r}+x+d_1, d'> \\
&= \sum_{r'\geq x;d'>0} t_{d_2;r',d'} e^{iK\frac{2x-2r'}{3}} |K, r'+d_1, d'> \\
&\quad + \sum_{r'>x;d'>0} t_{d_2;r',d'} e^{iK(\frac{2r'-2x}{3})} |K, -r'+2x+d_1, d'> \\
&= \sum_{r'\geq x;d'>0} t_{d_2;r',d'} \underbrace{e^{iK\frac{d_2-d'-2r'}{3}} |K, r'+d_1, d'>}_{III.\alpha} \\
&\quad + \sum_{r'>x;d'>0} t_{d_2;r',d'} \underbrace{e^{iK\frac{2r'+d'-d_2}{3}} |K, -r'+2x+d_1, d'>}_{III.\beta}.
\end{aligned}
$$

For $III.\alpha$ one ends with

$$
\begin{aligned}
.. &= \sum_{r'\geq\frac{d_2-d'}{2},d'} t_{d_2;r',d'} e^{iK\frac{d_2-d'-2r'}{3}}
\begin{cases}
|K, r'+d_1, d'> \\
\text{for } r'+d_1>0 \\
-|K, -r'-d_1, d'+r'+d_1> \\
\text{for } r'+d_1<0 \wedge d'+r'+d_1>0 \\
|K, d', -d'-r'-d_1> \\
\text{for } r'-d_1<0 \wedge d'+r'+d_1<0
\end{cases} \\
&= \sum_{r'\geq\frac{d_2-d'}{2},d'} t_{d_2;r',d'} e^{iK\frac{d_2-d'-2r'}{3}}
\begin{cases}
|K, r'+d_1, d'> \\
\text{for } -d_1<r' \\
-|K, -r'-d_1, d'+r'+d_1> \\
\text{for } -d_1-d'<r'<-d_1 \\
|K, d', -d'-r'-d_1> \\
\text{for } r'<-d'-d_1
\end{cases}
\end{aligned}
$$

and for $III.\alpha$ with

$$.. = \sum_{r'>\frac{d_2-d'}{2},d'} t_{d_2;r',d'} e^{iK\frac{2r'+d'-d_2}{3}} \begin{cases} |K,-r'+2x+d_1,d'> \\ \text{fuer } -r'+2x+d_1>0 \\ -|K,r'-2x-d_1,d'+d_1+2x-r'> \\ \text{for } -r'+2x+d_1<0 \wedge d'-r'+2x+d_1>0 \\ |K,d',-2x-d_1+r'-d'> \\ \text{for } -r'+2x+d_1<0 \wedge d'-r'+2x+d_1>0 \end{cases}$$

$$= \sum_{r'>\frac{d_2-d'}{2},d'} t_{d_2;r',d'} e^{iK\frac{2r'+d'-d_2}{3}} \begin{cases} |K,-r'+d_2-d'+d_1,d'> \\ \text{for } r'<d_1+d_2-d' \\ -|K,r'+d'-d_1-d_2,-r'+d_1+d_2> \\ \text{for } d_1+d_2-d'<r'<d_1+d_2 \\ |K,d',r'-d_1-d_2> \\ \text{for } r'>d_1+d_2 \end{cases}$$

A.3 The action of $H_3|_3$

is

$$H_3|r,r+d_1,r+d_1+d_2>=\sum_{r',d_1',d_2'} t_{d_1,d_2;r',d_1',d_2'}|r+r',r+r'+d_1',r+r'+d_1'+d_2'> . \tag{A.9}$$

The notation is always correct. So only the symmetry of the hopping amplitudes can be exploitet, which read

$$\begin{aligned} t_{d_1,d_2;r',d_1',d_2'} &= t_{d_2,d_1;-r'+2x,d_2',d_1'} \\ \text{or} \qquad t_{d_1,d_2;r'+x,d_1',d_2'} &= t_{d_2,d_1;-r'+x,d_2',d_1'} \\ \text{with} \qquad x &= \frac{1}{2}\left(d_1-d_1'+d_2-d_2'\right) . \end{aligned}$$

The action on the momentum state gives

$$\begin{aligned} & H_3|k,d_1,d_2> \\ = & \sum_{r',d_1',d_2'} t_{d_1,d_2;r',d_1',d_2'} e^{iK(r+\frac{2d_1+d_2}{3})}|r+r',r+r'+d_1',r+r'+d_1'+d_2'> \\ = & \sum_{r',d_1',d_2'} t_{d_1,d_2;r',d_1',d_2'} e^{iK(-r'+\frac{2(d_1-d_1')+d_2-d_2'}{3})} e^{ik(r+\frac{2d_1'+d_2'}{3})}|r,r+d_1',r+d_1'+d_2'> \\ = & \sum_{r',d_1',d_2'} t_{d_1,d_2;r',d_1',d_2'} e^{iK(-r'+\frac{2x+d_1-d_1'}{3})}|K,d_1',d_2'> . \end{aligned}$$

The symmetry of the hopping amplitudes is used by restating the sum over r' by $y = -r' + x$

$$
\begin{aligned}
&= \sum_{y,d_1',d_2'} t_{d_1,d_2;-y+x,d_1',d_2'} e^{iK(y+\frac{-x+d_1-d_1'}{3}} |K, d_1', d_2'> \\
&= \sum_{y\leq 0,d_1',d_2'} t_{d_1,d_2;-y+x,d_1',d_2'} e^{iK(y+\frac{-x+d_1-d_1'}{3})} |K, d_1', d_2'> \\
&\quad + \sum_{y>0,d_1',d_2'} t_{d_1,d_2;-y+x,d_1',d_2'} e^{iK(y+\frac{-x+d_1-d_1'}{3})} |K, d_1', d_2'> \\
&= \sum_{y\leq 0,d_1',d_2'} t_{d_1,d_2;-y+x,d_1',d_2'} e^{iK(y+\frac{-x+d_1-d_1'}{3})} |K, d_1', d_2'> \\
&\quad + \sum_{y<0,d_1',d_2'} t_{d_2,d_1;-y+x,d_2',d_1'} e^{iK(-y+\frac{-x+d_1-d_1'}{3})} |K, d_1', d_2'> \\
&= \sum_{r'\geq x,d_1',d_2'} t_{d_1,d_2;r',d_1',d_2'} e^{iK(-r'+x+\frac{-x+d_1-d_1'}{3})} |K, d_1', d_2'> \\
&\quad + \sum_{r'>x,d_1',d_2'} t_{d_2,d_1;r',d_2',d_1'} e^{iK(r'-x+\frac{-x+d_1-d_1'}{3})} |K, d_1', d_2'> .
\end{aligned}
$$

The final result is

$$
\begin{aligned}
&H_3|k, d_1, d_2> \\
= &\sum_{r'\geq\frac{d_1-d_1'+d_2-d_2'}{2};d_1',d_2'>0} t_{d_1,d_2;r',d_1',d_2'} e^{iK(-r'+\frac{2(d_1-d_1')+d_2-d_2'}{3})} |K, d_1', d_2'> \\
+ &\sum_{r'>\frac{d_1-d_1'+d_2-d_2'}{2};d_1',d_2'>0} t_{d_2,d_1;r',d_2',d_1'} e^{iK(r'-\frac{d_1-d_1'+2(d_2-d_2')}{3})} |K, d_1', d_2'> .
\end{aligned}
$$

Bibliography

[1] E. Dagotto and T.M. Rice, Science **271**, 618 (1996)

[2] J. Orenstein and A.J. Millis, *Advances in the Physics of High-Temperature Superconductivity*, Science **288**, 468 (2000)

[3] A.A. Nersesyan and A.M. Tsvelik, Phys. Rev. Lett., **78** 3939 (1997)

[4] G.S. Uhrig and M. Grüninger, *Das Wechselspiel magnetischer Anregungen in Spinflüssigkeiten*, Physik Journal 2 (2003) Nr. 1

[5] M. Grüninger, M. Windt, E. Benckiser, T.S. Nunner, K.P. Schmidt, G.S. Uhrig and T. Kopp, *Optical Spectroscopy of Low-Dimensional Quantum Spin Systems*, Adv. Sol. Stat.Phys. **43**, 95-112 (2003)

[6] P.A. Fleury and R. Loudon , Phys. Rev., **166**, (1968) 514

[7] B.S. Shastry and B.I. Shraiman, Phys. Rev. Lett., **65** (1990) 1068

[8] K.P. Schmidt, C. Knetter and G.S. Uhrig, *Raman response in antiferromagnetic two-leg $S = 1/2$ Heisenberg ladders*, Europhys. Lett. **56** (6), pp. 877-883 (2001)

[9] G.S. Uhrig and B. Normand, *Magnetic Properties of $(VO)_2P_2O_7$ from Frustrated Interchain Coupling*, Phys. Rev. B **58**, R14705 (1998)

[10] C. Knetter and G.S. Uhrig, *Perturbation Theory by Flow Equations: Dimerized and Frustrated $S = 1/2$ Chain*, Eur. Phys. J B **13**, 209 (200)

[11] Ch. Knetter, K.P. Schmidt, G.S. Uhrig, *The Structure of Operators in Effective Particle-Conserving Model*, Journal of Physics A **36**, 7889 (2003)

[12] S. Trebst et al., Phys. Rev. Lett. **85**, 4373 (2000)

[13] W. Zheng et al., Phys. Rev. B **63**, 144410 (2001)

[14] W. Zheng et al., Phys. Rev. B **63**, 144411 (2001)

[15] F. Wegner, *Flow-equations for Hamiltonians*, Ann. Physik **3** (1994) 77-91

[16] Ch. Knetter, *Perturbative Continuous Unitary Transformations: Spectral Properties of Low Dimensional Spin Systems*, Universität zu Köln, Juni 2003

[17] A. Mielke, *Flow equations for band-matrices*, Eur. Phys. J. B **5**, 605 (1998)

[18] Ch. Knetter, K.P. Schmidt, G.S. Uhrig, *High Order Perturbation Theory for Spectral Densities of Multi-Particle Excitations: $S = 1/2$ Two-Leg Heisenberg Ladder*, Eur. Phys. J. B **36**, 525 (2004)

[19] K.P. Schmidt und G.S. Uhrig, *Excitations in one-dimensional S=1/2 quantum antiferromagnets*, Phys. Rev. Lett. **90**, 227204 (2003)

[20] K.P. Schmidt, C. Knetter and G.S. Uhrig, *Novel Extrapolation for Strong Coupling Expansions*, Acta Physica Polonica B **34**, 1481 (2003)

[21] K.P. Schmidt, H. Monien and G.S. Uhrig, *Rung-singlet phase of the $S = 1/2$ two-leg spin-ladder with four-spin cyclic exchange*, Physical Review B **67**, 184413 (2003)

[22] K.P. Schmidt, *Spectral Properties of Quasi-One-Dimensional Quantum Antiferromagnets*, Universität zu Köln, Juni 2004

[23] C. Knetter, K.P. Schmidt, M. Grüninger and G.S. Uhrig, *Fractional and Integer Excitations in Quantum Antiferromagnetic Spin* 1/2 *Ladders*, Phys. Rev. Lett. **87**, 167204 (2001)

[24] T.S. Nunner, P. Brune, T. Kopp, M. Windt, and M. Grüninger, Phys. Rev. B **66**, 180404 (2002)

[25] J. Lorenzana and G.A. Sawatzky, Phys. Rev. Lett. **74**, 1867 (1995)

[26] J. Lorenzana and G.A. Sawatzky, Phys. Rev. B **52**, 9576 (1995)

[27] M. Grüninger, M. Windt, T. Nunner, C. Knetter, K.P. Schmidt, G.S. Uhrig, T. Kopp, A. Freimuth, U. Ammerahl, B. Büchner and A. Revcolevschi, *Magnetic excitations in two-leg spin* 1/2 *ladders: experiment and theory*, Journal of Physics and Chemistry of Solids **63**, 2335 (2002)

[28] T.S. Nunner, P. Brune, T. Kopp, M. Windt and M. Grüninger, Acta Phys. Pol. B **34**, 1545 (2003)

[29] R. Haydock, V. Heine and M.J. Kelly, *Electronic structure based on the local atomic environment for tight-binding bands*, J Phys C: Solid State Phys. Vol 5 (1972)

[30] J. Stoer and R. Bulirsch, *Numerische Mathematik 2*, 4th edition Springer (2000)

[31] D.G. Pettifor and D.L. Wearie, *The Recursion Method; Application to Many-Body Dynmics*, Vol. **58** of Springer Series in Solid State Sciences (1984)

[32] D.M. Bylander and J.J. Rehr, *Recursion method for the extendet impurity problem*, J. Phys. C Solid St. Phys. **13**,4157-74 (1980)

[33] C.H. Hodges, *Van Hove singularities and continued fraction coefficients*, J. Physique Lett. **38**, L187- L189 (1977)

[34] G.S. Uhrig und H.J. Schulz, *Magnetic Excitation Spectrum of Dimerized Antiferromagnetic Chains*, Phys. Rev. B **54**, R9624 (1996)

[35] K.P. Schmidt, C. Knetter, M. Grüninger und G.S. Uhrig, *Charge order induced sharp Raman peak in* $Sr_{14}Cu_{24}O_{41}$, Phys. Rev. Lett. **90**, 167201 (2003)

Erklärung Hiermit erkläre ich, dass die vorliegende Arbeit von mir selbständig angefertigt wurde und ausser den angegebenen Quellen keine weiteren Hilfsmittel verwendet wurden.

Sebastian Kirschner

Danksagung Ich möchte mich bei Herrn Priv.-Doz. Dr. Götz S. Uhrig für die Vergabe und die Betreuung der Diplomarbeit und die konstruktiven Diskussionen bedanken. Ein besonderes Dankeschön geht auch an Herrn Prof. Dr. E. Müller-Hartmann für seine Bereitschaft, Herrn Dr. Götz S. Uhrig im Diplomkolloquium zu verteten und an Herrn Prof. Dr. M. Braden als Zweitkorrektor. Herrn Kai Schmidt und Herrn Carsten Aits danke ich für das Korrekturlesen meiner Arbeit. Dank für die nette Atmosphäre und viele interessante Stunden geht an die Doktoranden der Arbeitsgruppe.